

by

K. H. Coats
 INTERCOMP Resource Development
 and Engineering, Inc.

© Copyright 1977, American Institute of Mining, Metallurgical, and Petroleum Engineers, Inc.

This paper was presented at the 52nd Annual Fall Technical Conference and Exhibition of the Society of Petroleum Engineers of AIME, held in Denver, Colorado, Oct. 9-12, 1977. The material is subject to correction by the author. Permission to copy is restricted to an abstract of not more than 300 words. Write 6200 N. Central Expy., Dallas, Texas 75206.

ABSTRACT

This paper describes and partially evaluates an implicit, three-dimensional geothermal reservoir simulation model. The evaluation emphasizes stability or time-step tolerance of the implicit finite-difference formulation. In several illustrative multiphase flow problems, the model stably accommodated time steps corresponding to grid block saturation changes of 80-100% and grid block throughput ratios the order of 10^8 . This compares to our experience of limits of 3 to 10% saturation change and roughly 20,000 throughput ratio with semi-implicit oil and geothermal reservoir models.

The illustrative applications shed some light on practical aspects of geothermal reservoir behavior. Applications include single- and two-phase single-well behavior, fractured-matrix reservoir performance and well test interpretation, and extraction of energy from fractured hot dry rock. Model stability allows inclusion of formation fractures and wellbores as grid blocks.

An analytical derivation is presented for a well deliverability reduction factor which can be used in simulations using large grid blocks. The factor accounts for reduced deliverability due to hot water flashing and steam expansion accompanying pressure decline near the well.

References and illustrations at end of paper.

INTRODUCTION

This paper describes a numerical model for simulating geothermal well or reservoir performance. The model is considerably more general than any described in the literature to date. It treats transient, three-dimensional, single- or two-phase fluid flow in normal heterogeneous or fractured-matrix formations. Both conductive and convective heat flow are accounted for and fluid states in the reservoir can range from undersaturated liquid to two-phase steam-water mixtures to superheated steam. Aquifer water influx and heat source/sink terms necessary in simulating free convection cells are included in the model formulation.

The primary purpose of the work described here was evaluation of the capability of an implicit model formulation. Our experience with semi-implicit simulation of petroleum and geothermal reservoirs has shown time step restrictions related to conditional stability. In multiphase flow problems, the maximum tolerable time step size generally corresponds to a maximum of 3 to 10 percent saturation change in any grid block in one time step. In some steamflood and geothermal simulations, we have found this to result in very small time steps and correspondingly high computing costs. This work was performed with the hope that the implicit model formulation would give unconditional stability with no time step restriction other than that imposed by time truncation error.

Calculated results are presented for a variety of geothermal well and reservoir illustrative problems. Emphasis in connection with these results is placed on the stability or time step tolerance of the model. However, the applications are also intended to shed some light on practical aspects of geothermal reservoir behavior.

Following description of the implicit model formulation, the paper presents applications including single-well deliverability under two-phase flow conditions, depletion of a fractured-matrix formation with boiling, drawdown test interpretation in single-phase, fractured-matrix formations, and heat extraction from artificially fractured hot dry rock. An analytical expression is derived to represent the effective transient productivity index of a well which experiences hot water flashing due to pressure drawdown from an exterior radius where steam saturation may be zero or small.

We have applied the model extensively in simulation of natural convection cells with zero porosity (hard rock) grid block definition above and below the formation. This definition eliminates the erroneous imposition of constant temperature boundaries at the top and bottom of the convection cell common in many reported studies of natural convection. Another application simulated development over geologic time of a superheated (Geyser's type) reservoir from an early time of magma or heat source intrusion beneath an initial normal gradient cold water aquifer. These natural convection type applications are omitted here due to the significant length of the paper. Some of this convection work is reported in a recent paper [1].

MODEL DESCRIPTION

The model consists of two equations expressing conservation of mass of H_2O and conservation of energy. These equations account for three-dimensional, single- or two-phase fluid flow, convective and conductive heat flow in the reservoir and conductive heat transfer between the reservoir and overlying and underlying strata. The phase configuration at any time can vary spatially through the formation from single-phase undersaturated water to two-phase steam-water mixture to single-phase superheated steam.

The equations represent water influx from an aquifer extending beyond the reservoir grid using the Carter-Tracy [2] or simpler approximations. Heat source and sink terms in the equations are useful in imposing temperature and/or heat flux boundary conditions in simulation of natural convection. The model equations do not account for the presence of inert gases or for varying concentration and precipitation of dissolved salts.

The model applies to reservoir grids including one-dimensional, two-dimensional radial-z, x-z or x-y and three-dimensional, either x-y-z Cartesian or r- θ -z cylindrical. In the r-z and r- θ -z case, the wellbore of a well at $r = 0$ can be included in the grid, resulting in enhanced stability and accuracy as discussed below. The r-z grid can be used in simulating a sector of a fractured-matrix reservoir with the horizontal and vertical fractures represented by grid blocks. The grid can include blocks of zero porosity representing hard rock, with no pressure calculated, and blocks of 100% porosity representing either fractures or wellbores.

The mass balance on H_2O combines in a single equation the steam-phase and liquid water-phase mass balance equations. This combination was proposed in our early steam-flood work [3] to eliminate difficulties in handling the mass transfer term. The energy balance is the First Law of Thermodynamics applied to each grid block. The grid block is an open system with fixed boundaries. With potential and kinetic energy terms ignored, the energy balance states that (enthalpy flow rate in) - (enthalpy flow rate out) = rate of gain of internal energy in the grid block. For some reason, considerable confusion exists in the literature regarding this energy balance. Enthalpy is $U + pv$ where U is internal energy. Many modelling papers ignore the pv term, in which case the energy balance erroneously becomes (net flow rate of internal energy into the grid block = rate of gain of internal energy in the block). A recent paper [4] uses an erroneous energy balance stating (net flow rate of enthalpy into the grid block = rate of gain of enthalpy in the block).

The two model equations are*

$$\Delta [T_w (\Delta p_w - \gamma_w \Delta z) + T_g (\Delta p_g - \gamma_g \Delta z)] - q = \frac{V}{\Delta t} \delta (\phi \rho_w S_w + \phi \rho_g S_g) \quad (1a)$$

$$\Delta [T_w H_w (\Delta p_w - \gamma_w \Delta z) + T_g H_g (\Delta p_g - \gamma_g \Delta z)] + \Delta (T_c \Delta T) - q_{HL} - q_H = \frac{V}{\Delta t} \delta (\phi \rho_w S_w U_w + \phi \rho_g S_g U_g) + (1-\phi) (\rho C_p)_R T \quad (1b)$$

For a given grid block (i, j, k) , all terms in these equations are single-valued functions of $(T, S_g, p)_{i, j, k}$ and (T, S_g, p) in the six neighboring grid blocks $(i+1, j, k)$, $(i, j+1, k)$, $(i, j, k+1)$. Thus, transposing the right-hand sides, we can write Equations (1) simply as

*See Nomenclature for definition of terms.

$$F_1(\underline{x}) = 0 \quad (2)$$

$$F_2(\underline{x}) = 0$$

where \underline{x} represents the vector of the above listed 21 unknowns.

Following the totally implicit procedure described by Blair and Weinaug [5], we apply the Newton-Raphson iterative method to (2) as

$$F_1(\underline{x}) \cong F_1(\underline{x}^l) + \sum_{i=1}^{21} (\partial F_1 / \partial x_i)^l \delta x_i = 0 \quad (3)$$

$$F_2(\underline{x}) \cong F_2(\underline{x}^l) + \sum_{i=1}^{21} (\partial F_2 / \partial x_i)^l \delta x_i = 0$$

where we temporarily use x_i to denote the 21 unknowns and superscript l denotes latest iterate value. The operator δ in Equations (1) denotes change over time step while δ in Equations (3) denotes change over the coming iteration. The approximation $\delta x_i \cong x_{i,n+1} - x_i^l$ becomes increasingly exact as we near convergence.

The partial derivatives in Equations (3) are all evaluated at latest iterate values of x_i . The functions F_1, F_2 involve three different types of terms: right-hand sides (accumulation terms), sink/source terms and interblock flow terms. Differentiation of accumulation terms is straightforward. The heat loss term and its derivative is evaluated as described in Reference [3]. The well injection/production terms and their derivatives are evaluated as described in some detail below. The interblock flow terms are evaluated as follows: Relative permeabilities and enthalpies are evaluated at upstream grid block conditions, interblock ρ/μ and γ values are evaluated as arithmetic averages of their values in the two grid blocks. Water phase pressure p_w is expressed as $p - P_c$ where p is gas pressure and capillary pressure P_c is a single-valued function of S_g .

For all $N_x N_y N_z$ grid blocks taken together, Equations (3) are $2N_x N_y N_z$ equations in $3N_x N_y N_z$ unknowns, $(\delta T, \delta S_g, \delta p)$ for each grid block. Only two of these three unknowns in each block are independent. If the block contains undersaturated water or superheated steam, $\delta S_g = 0$ and $\delta T, \delta p$ are the block's two unknowns. If the block is saturated, two-phase, then temperature $T = T_s(p)$ and δT is $(dT/dp)_s \delta p$ where subscript s denotes the saturated condition.

Equations (3) can be written for each grid block in the form

$$\Delta(T_{11}\Delta P_1) + \Delta(T_{12}\Delta P_2) + R_1 = C_{11}P_1 + C_{12}P_2 \quad (4)$$

$$\Delta(T_{21}\Delta P_1) + \Delta(T_{22}\Delta P_2) + R_2 = C_{21}P_1 + C_{22}P_2$$

where P_1 is either δT or δS_g and P_2 is δp . The terms R_1, R_2 are $F_1(\underline{x}^l), F_2(\underline{x}^l)$, respectively, in Equations (3). The $\Delta(TAP)$ type terms are not true Laplacians but rather are, as illustrated by the x -direction component

$$\Delta_x(T_x \Delta_x P) = T_{xi}^+ P_{i+1} + T_{xi}^0 P_i + T_{xi}^- P_{i-1}$$

where the center term T_{xi}^0 can be combined with the appropriate C_{ij} in Equation (4) and need not be stored. More simply, Equation (4) can be written

$$\Delta(TAP) + \underline{R} = \underline{CP} \quad (5)$$

where T and C are the 2×2 matrices T_{ij} , C_{ij} and \underline{R} and \underline{P} are column vectors. We use reduced band width direct solution [6] to solve Equation (5) for P_1, P_2 and obtain new iterate values as $p^{l+1} = p^l + \delta p$. Convergence is defined by

$$\begin{aligned} \text{Max} |\delta p_{ijk}| &\leq \epsilon_p \\ \text{Max} |\delta T_{ijk}| &\leq \epsilon_T \\ \text{Max} |\delta S_{gijk}| &\leq \epsilon_S \end{aligned} \quad (6)$$

where MAX denotes maximum over all grid blocks. We generally use tolerances of .1 psia, 1°F, 1% saturation and have not found sensitivity of results to tighter tolerances.

PVT TREATMENT

At saturated conditions, U_w, U_g, ρ_w, ρ_g are evaluated as single-valued functions of temperature from the Steam Tables [7]. U_w is assumed a single-valued function of temperature for undersaturated water. Density of undersaturated water is calculated as

$$\rho_w \cong \rho_{ws}(T) [1 + c_w(T)(p - p_s(T))] \quad (7)$$

where subscript s denotes saturation condition. The "compressibility" $c_w(T)$ is derived as follows. The Steam Tables [7] include a tabulation of $(v - v_s)$ for undersaturated water as a function of temperature and pressure, where v is specific volume, cubic feet per pound. The tabular values are fit well by the expression

$$v = v_s - s(T)(p - p_s(T))$$

where $s(T)$ is dependent only upon temperature as:

$T, ^\circ\text{F}$	$s(T) \times 10^5$
< 200	.0054
300	.0072
400	.0109
500	.0205
600	.065
660	.355

This equation can be written

$$\frac{1}{\rho_w} = \frac{1}{\rho_{ws}(T)} - \frac{s(T)\rho_{ws}(T)}{\rho_{ws}(T)}(p - p_s(T))$$

Since $s(T)\rho_{ws}(T)(p - p_s(T))$ is small in comparison to 1 (except at temperatures approaching 700°F), this equation can be written as Equation (7) where $c_w(T)$ is $s(T)\rho_{ws}(T)$.

For superheated steam, internal energy U_g and density ρ_g are approximated by

$$U_g \cong U_{gs}(p) + C_{p\text{steam}}(T - T_s(p)) \quad (8)$$

$$\rho_g \cong \rho_{gs}(p) \frac{T_s(p) + 460}{T + 460} \quad (9)$$

where specific heat $C_{p\text{steam}}$ is constant. Equation (9) is accurate in proportion to the constancy of steam z-factor from $p, T_s(p)$ to p, T . Water and steam phase viscosities are evaluated as single-valued functions of temperature equal to their respective saturated values. Enthalpies are

$$H_w = U_w + 144/778.2 p/\rho_w \quad (10)$$

$$H_g = U_g + 144/778.2 p/\rho_g$$

The model uses steam phase pressure as the pressure variable in all PVT relationships.

Porosity is calculated from

$$\phi = \phi_0(1 + c_r(p - p_0)) \quad (11)$$

where ϕ_0 is porosity at pressure p_0 and c_r is constant. Reservoir thermal conductivity may vary with spatial position, but is treated as independent of pressure, temperature and saturation. Formation rock heat capacity may vary with position but is independent of temperature. Overburden thermal conductivity and heat capacity are constants.

IMPLICIT AND SEMI-IMPLICIT ALLOCATIONS

OF WELL RATE AMONG LAYERS

Numerical simulation of most reservoir processes encounters the problem of representing production rates from wells located in grid blocks of large areal dimensions. The reservoir grid system consists of NZ vertical layers with the layers numbered from top to bottom as $k = 1, k = 2, \dots, k = NZ$. A producing well located in areal block (i, j) is perforated or open to flow in layers $k = k_1, k_1 + 1, \dots, k_2$. For example, NZ might be 8 and a well open in layers 3-7, ($k_1 = 3, k_2 = 7$). The wellbore radius is denoted by r_w . The grid blocks penetrated by the well are of dimensions $\Delta x, \Delta y, \Delta z_k$ where Δx and Δy are the areal dimensions. Assuming (a) $\Delta x \cong \Delta y$, (b) the well is located areally near the center of the grid block, (c) steady- or semi-steady-state radial flow in each grid block $\Delta x, \Delta y, \Delta z_k$ open to the well, (d) no vertical crossflow between open layers, we can derive from Darcy's law for single-phase flow of a unit mobility fluid ($k_r/\mu = 1$)

$$Q_k \cong \frac{2\pi(k\Delta z)_k}{\ln(r_e/r_w) + S}(p_k - p_{wbk}) \cong PI_k(p_k - p_{wbk}) \quad (12)$$

where

- Q_k = rate of radial flow of a unit mobility fluid in layer k from grid block to the wellbore, cubic feet/day,
- k_k = absolute permeability of layer k , md x 0.00633,
- Δz_k = layer thickness, feet,
- S = skin factor,
- r_e = $\sqrt{\Delta x \cdot \Delta y / \pi}$ = equivalent radius feet,
- p_k = pressure in grid block i, j, k at $r = r_e$, psia,
- p_{wbk} = flowing wellbore pressure opposite layer k , psia.

In practice, for the case where $r_e \gg r_w$, we assume p_k equal to the average grid block pressure calculated in the simulator and, for more rigor, replace S by $S - 1/2$ or $S - 3/4$ for steady- or semi-steady-state flow. PI_k denotes the coefficient in Equation (12), a layer productivity index in units of cubic feet/day-psi. All pressures p_k , P_{wbk} refer to points vertically centered in the thickness Δz_k .

In the geothermal reservoir case treated here, \bar{q} denotes the well target or desired production rate, and \bar{P}_{wb} denotes the minimum flowing wellbore pressure in layer k_t . If no tubing is in the well, then k_t would normally be specified as k_1 , the uppermost open layer. If tubing is in the perforated casing, then a minimum (bottomhole tubing) wellbore pressure may be specified at any layer, $k_1 \leq k_t \leq k_2$.

P_{wb} denotes the actual flowing wellbore pressure at the center of layer $k = k_t$ and q denotes the actual total well production rate, lbs H_2O per day. The flowing wellbore pressure in layer k is denoted by

$$P_{wbk} = P_{wb} + \Delta P_{wbk} \quad (13)$$

From Equations (12) and (13) the production rates of water phase, gas (steam) phase, total H_2O and enthalpy from layer k are

$$\begin{aligned} q_{wk} &= \alpha_{wk} (p_k - P_{wb} - \Delta P_{wbk}) \\ q_{gk} &= \alpha_{gk} (p_k - P_{wb} - \Delta P_{wbk}) \\ q_k &= q_{wk} + q_{gk} = \alpha_k (p_k - P_{wb} - \Delta P_{wbk}) \end{aligned} \quad (14)$$

$$q_{Hk} = q_{wk} H_{wk} + q_{gk} H_{gk}$$

where

$$\alpha_{wk} = PI_k (k_{rw} \rho_w / \mu_w)_k$$

$$\alpha_{gk} = PI_k (k_{rg} \rho_g / \mu_g)_k$$

$$\alpha_k = \alpha_{wk} + \alpha_{gk}$$

and ρ_w , ρ_g are phase densities in units of lbs H_2O per cubic foot.

As discussed above, the interblock flow rates and heat loss and conduction terms are all treated implicitly in the simulator described herein. If, in addition, the well sink or source terms are implicit, then the entire simulator is implicit. The logic and coding necessary for implicit well treatment is rather simple for the case of a well completed in a single layer of the reservoir grid. Implicit treatment can be extremely difficult for a producing well completed in several layers.

In this section we describe an implicit treatment for multilayer well completion and present several semi-implicit simplifications. Note that α_k in Equations (14) is a function of pressure, temperature and, due to relative permeabilities, saturation S_g . Enthalpies H_w , H_g are functions of pressure and temperature. Total well production rate q is the sum of q_k over layers $k_1 - k_2$ or

$$q = \sum \alpha_k (p_k - \Delta P_{wbk}) - P_{wb} \sum \alpha_k \quad (15)$$

where the summation term Σ denotes summation from k_1 to k_2 . Rearranging Equation (15) gives

$$P_{wb} = (\sum \alpha_k (p_k - \Delta P_{wbk}) - \bar{q}) / \sum \alpha_k \quad (16)$$

as the flowing bottomhole wellbore pressure at center of layer k_t necessary to produce the well target rate \bar{q} lbs H_2O per day. The well is on deliverability if P_{wb} from Equation (16) is less than the specified minimum value \bar{P}_{wb} . In any event, the production rates of water, steam and H_2O are given by Equations (14a) - (14c) with P_{wb} equal to the larger of \bar{P}_{wb} and the value given by Equation (16).

Implicit well treatment requires that water phase production rate given by Equation (14a) be expressed as

$$\begin{aligned} q_{wk} &= q_{wk}^{\ell} + \sum \frac{\partial q_{wk}}{\partial T_m} \delta T_m + \sum \frac{\partial q_{wk}}{\partial S_{gm}} \delta S_{gm} \\ &\quad + \sum \frac{\partial q_{wk}}{\partial p_m} \delta p_m + \frac{\partial q_{wk}}{\partial P_{wb}} \delta P_{wb} \end{aligned} \quad (17)$$

where summation here is over m from k_1 to k_2 , superscript ℓ denotes evaluation at latest iterate values of all variables, all partial derivatives are evaluated at latest iterate conditions, δT_m , δS_{gm} , δp_m are changes in layer m over the coming iteration and q_{wk} is an approximation to the end-of-time step (implicit) value $q_{wk,n+1}$. The gas

phase production rate q_{gk} in Equation (14b) is represented in an analogous fashion. If the producing cell is two-phase ($0 < S_g < 1$), then $\delta T_m = (dT/dp)_s \delta p_m$ where $(dT/dp)_s$ is the slope of saturated temperature vs. saturated pressure at the latest iterate pressure value. If the producing cell is single-phase ($S_g = 0$ or $S_g = 1$), then $\delta S_g = 0$. Thus only two of the three unknowns δT_m , δS_{gm} , δp_m are independent in any case.

The implicit expressions for q_{wk} , q_{gk} , q_{Hk} of type shown in Equation (17) introduce one additional unknown δp_{wb} for each well. The additional required equation corresponding to this unknown is the constraint equation stating that the summation over k $\Sigma(q_{wk} + q_{gk})$ equals target well rate \bar{q} lbs H₂O/day:

$$\sum_{k=k_1}^{k_2} \left\{ \sum_{m=k_1}^{k_2} \left[\left(\frac{\partial q_{wk}}{\partial T_m} + \frac{\partial q_{gk}}{\partial T_m} \right) \delta T_m + \left(\frac{\partial q_{wk}}{\partial S_{gm}} + \frac{\partial q_{gk}}{\partial S_{gm}} \right) \delta S_{gm} + \left(\frac{\partial q_{wk}}{\partial p_m} + \frac{\partial q_{gk}}{\partial p_m} \right) \delta p_m \right] + \left(\frac{\partial q_{wk}}{\partial p_{wb}} + \frac{\partial q_{gk}}{\partial p_{wb}} \right) \delta p_{wb} \right\} = 0 \quad (18)$$

This Equation (18) guarantees that $\Sigma(q_{wk} + q_{gk}) = \bar{q}$ because q_{wk}^l , q_{gk}^l are calculated using latest iterate values in Equations (14) and p_{wb}^l from Equation (16). That is, $\Sigma(q_{wk}^l + q_{gk}^l) = \bar{q}$. If the well is on deliverability (i.e. p_{wb}^l from Equation (16) is $\leq \bar{p}_{wb}$), then $\delta p_{wb} = 0$ and Equation (18) is not required.

The implicit well treatment consisting of Equations (17) (and similar equations for q_{gk} , q_{Hk}) and (18) is extremely difficult to implement due to the derivatives involved. The derivatives $\partial q_{wk}/\partial p_m$, $\partial q_{gk}/\partial S_{gm}$, etc., where $k \neq m$ arise from the wellbore pressure gradient term Δp_{wbk} which is $p_{wbk} - p_{wb}$. This term must be obtained by calculating the horizontal flow rates of water and steam phases from each open layer into the well, cumulating these flow rates upward from layers $k > k_t$, downward from layers $k < k_t$, performing an energy balance in each wellbore layer by flashing the total flowing stream to obtain quality, and then calculating density (psi/ft) in each wellbore layer by volumetrically averaging steam and water densities. At a given iteration, this calculation is laborious and iterative in itself.

A significant simplification results if we evaluate the term Δp_{wbk} in Equations (14) at time level n . This, of course, results in a semi-implicit well treatment and can result in a time step restriction or conditional stability. Using $\Delta p_{wbk,n}$ in Equations (14) and employing an implicit approach to the remaining terms, we have

$$q_{wk} = q_{wk}^l + \frac{\partial q_{wk}}{\partial T_k} \delta T_k + \frac{\partial q_{wk}}{\partial S_{gk}} \delta S_{gk} + \frac{\partial q_{wk}}{\partial p_k} \delta p_k + \frac{\partial q_{wk}}{\partial p_{wb}} \delta p_{wb} \quad (19)$$

and similar equations for q_{gk} , q_{Hk} , where q_{wk}^l and all partial derivatives are evaluated at latest iterate conditions (except for $\Delta p_{wbk,n}$). The impact of taking Δp_{wbk} at time level n is that all derivatives of type $\partial Y_k/\partial X_m$ are zero unless $m = k$. Again, the constraint Equation (18) applies (with $\partial Y_k/\partial X_m = 0$ if $m \neq k$) if the well is not on deliverability ($p_{wb}^l > \bar{p}_{wb}$) and Equation (18) is inactive with $\delta p_{wb} = 0$ if the well is on deliverability ($p_{wb}^l = \bar{p}_{wb}$).

A further simplification, for the case where the well is not on deliverability, is

$$q_{wk} = q_{wk}^l + q_k^l \left(\frac{\partial f_{wk}}{\partial T_k} \delta T_k + \frac{\partial f_{wk}}{\partial p_k} \delta p_k + \frac{\partial f_{wk}}{\partial S_{gk}} \delta S_{gk} \right) + \frac{\partial q_{wk}}{\partial p_k} \delta p_k + \frac{\partial q_{wk}}{\partial p_{wb}} \delta p_{wb} \quad (20)$$

where $\partial q_{wk}/\partial p_k$ is simply α_{wk} and f_{wk} is mass fractional flow of water phase from layer k ,

$$f_{wk} = \alpha_{wk} / (\alpha_{wk} + \alpha_{gk}) \quad (21)$$

This simplification automatically holds constant over the coming iteration the q_k^l lbs H₂O/day from each layer, as well as the sum $\Sigma(q_{wk}^l + q_{gk}^l) = \bar{q}$. This constancy of q_k^l eliminates the need for terms involving δS_{gk} , δT_k in the constraint Equation (18) and the constraint equation becomes simply

$$\Sigma \left(\frac{\partial q_{wk}}{\partial p_k} + \frac{\partial q_{gk}}{\partial p_k} \right) \delta p_k + \Sigma \left(\frac{\partial q_{wk}}{\partial p_{wb}} + \frac{\partial q_{gk}}{\partial p_{wb}} \right) \delta p_{wb} = 0 \quad (22)$$

or

$$\Sigma (\alpha_{wk} + \alpha_{gk}) \delta p_k = [\Sigma (\alpha_{wk} + \alpha_{gk})] \delta p_{wb} \quad (23)$$

Thus the constraint equation involves only pressures and if a single-variable pressure equation is solved in a simulator, then Equation (23) is compatible in that no saturation unknowns appear. We used this latter type of constraint equation four years ago in a black oil coning simulation and found that addition of the δp_{wb} unknown considerably improved stability and increased time step size.

If the well is on deliverability, no constraint equation or additional variable δp_{wb} is involved and the simplification of evaluating Δp_{wbk} at time level n is generally satisfactory in geothermal simulations. The incorporation of terms of type $\partial Y_k / \partial X_m$ where $m \neq k$ in expressions for q_{wk} , q_{gk} , q_{Hk} or incorporation of the constraint equation is often difficult from a coding point of view. The difficulty is minimized if z -line SOR or vertical-plane block SOR or direct solution is used, but even in these cases the storage and/or computing time requirements for many-well problems can rise appreciably. If the well is on deliverability, then the first simplification of $\Delta p_{wbk,n}$ requires on $\partial Y_k / \partial X_k$ derivatives and no constraint equation applies. Therefore, we use this simplification for the deliverability case.

If the well is not on deliverability, we use a simplification even more explicit than those described above. We express

$$q_{wk} = q_{wk}^l + q_k^l \left(\frac{\partial f_{wk}}{\partial T_k} \delta T_k + \frac{\partial f_{wk}}{\partial S_{gk}} \delta S_{gk} + \frac{\partial f_{wk}}{\partial p_k} \delta p_k \right) \quad (24a)$$

$$q_{gk} = q_{gk}^l + q_k^l \left(\frac{\partial f_{gk}}{\partial T_k} \delta T_k + \frac{\partial f_{gk}}{\partial S_{gk}} \delta S_{gk} + \frac{\partial f_{gk}}{\partial p_k} \delta p_k \right) \quad (24b)$$

$$q_{Hk} = q_{wk}^l \left(\frac{\partial H_{wk}}{\partial T_k} \delta T_k + \frac{\partial H_{wk}}{\partial p_k} \delta p_k \right) + q_{gk}^l \left(\frac{\partial H_{gk}}{\partial T_k} \delta T_k + \frac{\partial H_{gk}}{\partial p_k} \delta p_k \right) + H_{wk}^l \delta q_{wk} + H_{gk}^l \delta q_{gk} \quad (24c)$$

where q_{wk}^l and q_{gk}^l are computed from Equations (14) using $\Delta p_{wbk,n}$ and p_{wb}^l from Equation (16). Thus, $\Sigma (q_{wk}^l + q_{gk}^l) = \bar{q}$. The derivatives $\partial f_{wk} / \partial T_k$, etc., are evaluated at latest iterate conditions. This simplification runs the risk of pressure instability since no $\partial q_{wk} / \partial p_k = \alpha_{wk}$, etc., terms are used. This instability increases as well productivity index PI increases and as rate \bar{q} decreases. In two-dimensional areal calculations, no such instability exists since there is no pressure allocation among layers. In many three-dimensional and two-dimensional cross-sectional problems, the PI is sufficiently low that the instability is not significant. In many radial- z single-well problems, the instability is severe and we return to implicit procedures.

In radial- z single-well problems, we achieve implicit well treatment by simply incorporating the wellbore in the reservoir grid system. The result of this inclusion is an even more rigorous well treatment than the implicit treatment described in Equations (17) - (18). For inclusion of the wellbore results in transient mass and energy balances applied within the wellbore. Also, reverse flow in any layers from wellbore to the formation is automatically modelled whereas this injection in a producing well is very difficult to account for if the wellbore is not modeled by inclusion in the grid. An apparent disadvantage of wellbore modelling is the very small volume grid blocks giving rise to very large throughput ratios (defined below) for reasonable time step sizes. Our hope at the outset of this work was that the implicit treatment throughout the wellbore and reservoir would eliminate instabilities regardless of very high throughput ratios.

The multiphase flow vertically within or laterally from the column of wellbore grid blocks cannot be modeled by the usual multiphase Darcy flow expressions. The large gas-liquid density difference and high effective vertical "permeability" of the wellbore results in domination by gravity forces even at very high producing rates. This gravity dominance gives low calculated steam saturations in the wellbore resulting in a liquid pressure gradient and high back pressure on the lower formation. At normal rates of geothermal wells, the Reynolds number is so high that assumption of fully developed turbulent flow in the wellbore is usually a good one and assumption of no-slip two-phase flow is an even better one. This no-slip condition is equivalent to volumetric fractional flow equalling saturation.

We programmed this no-slip flow in lieu of usual Darcy flow logic for the wellbore. Alternatively, we could use the Darcy flow logic but calculate wellbore pseudo relative permeabilities which result in volumetric fractional flow $f_g = S_g$. This approach would

require two sets of pseudo relative permeabilities since gravity enters for vertical but not for lateral flow. The vertical wellbore effective permeability used in calculations described below was sufficiently large to hold viscous pressure drops over 500 feet of wellbore to less than 3 psi.

This inclusion of the wellbore in the grid system allows radial-z or r- θ -z simulation of the entire wellbore and overburden from the formation to the surface (well-head). A problem arises here in altering the no-slip wellbore two-phase flow calculation so that agreement is obtained with two-phase vertical pipe flow correlations. Apart from this problem, the model allows simulation of transient wellbore flow conditions and wellbore heat loss, in addition to the transient multiphase heat and fluid flow in the reservoir. Vertical grid definition in this case would extend from ground surface down to and through the permeable formation.

EFFECT OF STEAM FLASHING ON WELL DELIVERABILITY

A problem in use of Equations (14) arises even in an areal simulation where $NZ = 1$, $k = 1$ and $\Delta p_{wbk} = 0$. The mobilities and specific volumes in Equations (14) are generally evaluated at average (exterior) grid block conditions. If flashing of steam occurs between r_e and r_w , then Equations (14) can give considerable error since they do not account for the increasing volumetric flow rate (at constant mass flow rate) toward the well due to water flashing and steam expansion accompanying pressure decline.

Deliverability of a single layer can be corrected to account for water flashing and steam expansion by inserting a fraction f , equal to or less than 1, as

$$q = f(\alpha_w + \alpha_g)(p - p_{wb}) \quad (25)$$

where, as before, α_w and α_g are evaluated at known block average (exterior) conditions. The factor f is a calculable function of p_{wb} , p and S_{ge} where S_{ge} is gas saturation at $r = r_e$, which in turn is generally very close to average grid block saturation. Equation (25) presumes that the average grid block condition is saturated. The Appendix describes the calculation of f and gives a revision of Equation (25) for the case where the saturation point lies between r_w and r_e . The calculation of f ignores capillary pressure and assumes steady-state radial flow from pressure p at r_e to pressure p_{wb} at r_w .

In addition to p_{wb} , p and S_{ge} , f is also dependent upon the relative permeability curves. Therefore, a completely general representation of f is not possible. Figure 1 gives f as a function of p_{wb} , $p (= p_e)$ and S_{ge} for relative permeability curves

$$k_{rw} = [(S_w - S_{wc}) / (1 - S_{wc})]^{n_w} \quad (26a)$$

$$k_{rg} = k_{rgcw} [(S_g - S_{gc}) / (1 - S_{wc} - S_{gc})]^{n_g} \quad (26b)$$

with $S_{wc} = .2$, $S_{gc} = 0$, $n_w = n_g = 2$ and $k_{rgcw} = .5$.

Figure 1 shows that the deliverability reduction factor is 1 for minimal drawdowns ($p_e - p_{wb}$), decreases with increasing drawdown and, for a given drawdown, it increases with increasing grid block steam saturation, S_{ge} . The factor can reach values of .25 or lower for low S_{ge} , high drawdown and/or low reservoir pressure p_e . This means that deliverabilities calculated using Equation (14) can be erroneously high by a factor of four or more.

Comparison of Numerical Model and Analytical Deliverabilities

A radial test problem was used to compare the simulator's calculated deliverability with that of Equation (25). This problem was also used as a preliminary test of simulator stability and time-truncation error. Reservoir and fluid property data for this problem are given in Table 1. A 9x1 radial grid was employed with the well producing on deliverability against a wellbore pressure of 160 psia.

In the past, we have performed radial gridding by specifying r_w , r_e and an arbitrary first block "center" radius r_1 . Geometric block center spacing gives $r_i = \alpha r_{i-1}$ where i is r-direction grid block index. Thus, $r_N = \alpha^{N-1} r_1$ and $r_{N+1} = \alpha^N r_1$ where N is the number of radial reservoir grid blocks. Demanding that r_e be the log mean radius between r_N and r_{N+1} gives the equation

$$\frac{\alpha^{N-1} (\alpha - 1) r_1}{\ln \alpha} = r_e \quad (27)$$

which is solved for α by the Newton-Raphson technique. Generally r_1 values of at least 3 feet or more have been used to avoid excessively small grid blocks adjoining the wellbore.

In this work we retain the geometric spacing $r_i = \alpha r_{i-1}$ but eliminate the arbitrary specification of r_1 . Rather we invoke an imaginary radius r_0 within the wellbore in addition to radius r_{N+1} outside r_e and require r_w be the log mean radius of r_0 and r_1 and r_e be the log mean of r_N and r_{N+1} . This gives

$$\frac{(\alpha - 1)r_0}{\ln \alpha} = r_w \quad (28a)$$

$$\frac{\alpha^N (\alpha - 1)r_0}{\ln \alpha} = r_e \quad (28b)$$

and division of Equation (28b) by Equation (28a) gives a direct solution for α as

$$\alpha = (r_e/r_w)^{1/N} \quad (29)$$

Grid block boundary radii used to calculate block pore volumes are calculated as log mean values of adjacent block center radii. Table 1 gives the resulting block center and boundary radii for the case of nine radial increments. The pore volume of the first grid block is 22.27 RB corresponding to 500 feet of formation thickness.

The simulator was run in one-dimensional radial mode using constant 250-day time steps to 16,000 days. Zero capillary pressure was used and the well was on deliverability against the 160 psia flowing bottomhole pressure. The solid curve in Figure 2 shows the calculated flow rates, expressed per foot of formation thickness, vs. average formation steam saturation. This saturation is close to the exterior grid block 9 saturation, but was calculated as a volume weighted average of all blocks. Figure 2 shows an initial deliverability decline followed by a temporary increase. This behavior was unaffected by time step size, closure tolerances, number of radial blocks and inclusion or exclusion of heat conduction and heat loss in the calculation.

The dotted lines in Figure 2 show deliverability from the steady-state Equation (25) for $p_{wb} = 160$, $p = p_e = 251$. The agreement between model production rate and Equation (25) is good considering that

(a) the model used a closed exterior boundary, (b) the model is in a transient decline exhibiting semi-steady-state neither in pressure nor saturation, (c) Equation (25) assumes steady-state with an open exterior boundary. Further, the deliverability factor f varies from .3428 at $S_{ge} = 0$ to .78 at $S_{ge} = .5$ and the discrepancy between the two curves is much less than the error which would occur using Equation (25) with $f = 1$.

The one-dimensional radial test problem was run to a large time to reach steady-state with an exterior-block well injecting 400°F water at a bottomhole pressure of 251.08 psia at $r = r_e$. Following several time steps to 100 days to allow pressure in grid block 9 to fall below 251 psia (to activate the injection well), two 60,000-day time steps (these steps required 7 and 2 iterations) were taken. The steady-state flow rate calculated was 130,000 lbs H₂O/hour. Equation (37) gives for $p_{wb} = 160$, $p_e = 251$ and $S_{ge} = 0$ (corresponding to injection of saturated 100% liquid water),

$$q_{H_2O} = \frac{2\pi k \Delta z_I}{\ln \frac{r_e}{r_w}} = \frac{2\pi (100) (500) (.00633)}{\ln \frac{2000}{.25}}$$

$$= \frac{12,728 \text{ lbs}}{24 \text{ hr}} = 117,349 \text{ lbs/hr}$$

The discrepancy between 130,000 and 117,349 lbs/hour is believed due to the model's upstream weighting of mobilities as opposed to the integration of mobility in Equation (37). In any event, since $f = .3428$ for $p_e = 251$, $p_{wb} = 160$ and $S_{ge} = 0$, the discrepancy of about 13,000 lbs/hour is small in comparison with the error in using Equation (25) with no correcting f factor. Equations (14) used for an areal grid block of 2,000 feet equivalent exterior radius would give a deliverability of 343,000 lbs/hour. Use of the f factor and Equation (25) would give a calculated deliverability of 117,349 lbs/hour.

THROUGHPUT RATIO

Evaluation of any term in the interblock flow rates explicitly (at time level n) with respect to any of the dependent variables (p , T , S_g) in general will result in a conditional stability. This conditional stability takes the form of an expression giving a maximum time step. Use of a time step size exceeding this maximum will result in divergence of the calculations. The expression for maximum time step generally involves, at least in part, a throughput ratio defined in some manner.

One of the most severe instabilities in multiphase flow simulation is that arising from explicit evaluation of saturation-dependent relative permeabilities in the interblock transmissibilities. The throughput ratio that arises in analysis of this instability is

$$R_{Ti} = \frac{q_i \Delta t}{V_p S_i} \quad (30)$$

where i denotes phase (e.g., water, gas or oil), q_i is volumetric phase flow rate through the grid block, S_i is grid block saturation of phase i and V_p is grid block pore volume. Thus R_{Ti} is the ratio of total volume of phase i passing through the grid block in one time step divided by the volume of phase i in the block.

Actually, this ratio appears with a multiplier equal to fractional flow derivative, but we are not concerned here with detailed derivations or presentations of stability analysis results. As a practical matter, we have rated the stability of a multiphase flow formulation or model by the cruder ratio

$$R_T = \frac{q_v \Delta t}{V_p} \quad (31)$$

where q_v is total (all phases) volumetric flow rate through the grid block.

In the geothermal case we can express the above ratio in terms of total mass flow rate of H_2O and quality X of the flowing stream. Many of the results discussed below involve a well producing on deliverability at a flowing bottomhole pressure of 160 psia. Using corresponding water and steam densities of 55 and .355 lbs/cu.ft., respectively, we can express R_T as

$$R_T = 4.27(2.8X + .018)q\Delta t/V_p \quad (32)$$

where q is total mass flow rate in lbs H_2O /hour, Δt is time step in days and V_p is reservoir barrels (RB).

Our previous experience with a variety of semi-implicit isothermal and thermal simulators, producing under multiphase flow conditions, has indicated instability or time step restriction at throughput ratios in the range of 1,000 to 20,000. We will return to Equation (32) in connection with results discussed below.

TIME TRUNCATION ERROR AND STABILITY FOR ONE-DIMENSIONAL RADIAL PROBLEM

Time truncation error and model stability were examined in the one-dimensional radial case by repeating the 16,000-day run described above with time steps of 500, 1,000, 2,000, 4,000, 8,000 and 16,000 days. Table 2 shows the effect of time step size on calculated recovery, producing quality and rate at 4,000, 8,000 and 16,000 days. The time truncation error is quite acceptable for time steps up to 1,000 days.

All these runs converged each time step with two to three iterations per step except for the first step when steam saturation increased from zero to about .45 at the well and 0 - .39 at the 9th block. The first time step required 20-23 iterations, the 23 iterations corresponding to the 16,000-day time step run. The largest throughput ratio occurred for the 16,000-day time step which, from Equation (32), is

$$\begin{aligned} R_T &= 4.27(2.8(.0835) + \\ &\quad .018)(67,900)(16,000)/22.27 \\ &= 52.45 \times 10^6 \end{aligned}$$

This ratio is more than three orders of magnitude larger than the 20,000 ratios of our previous experience mentioned earlier. However, one-dimensional problems are generally poor tests or indicators of true model competence and ratios from two-dimensional results presented below will be given more emphasis.

TWO-DIMENSIONAL SINGLE-WELL PROBLEM RESULTS

We simulated the radial flow problem described in Table 1 using a two-dimensional 10 x 5 radial-z grid. The five layers were each 100 feet thick. The 10 radial grid blocks included the wellbore. Table 1 gives the grid block center radii, boundary radii and pore volumes calculated using Equation (29). Note that the first reservoir grid block has a center radius of only .40 feet and a pore volume of only 4.45 RB. The pore volume of each wellbore grid block is 3.5 RB so that the throughput ratio, Equation (32), becomes

$$R_T = 1.22(2.8Q + .018)q\Delta t \quad (33)$$

Rock capillary pressure was assumed negligible in this problem and a pseudo straight-line capillary pressure curve [8, 9] corresponding to layer thickness of 100 feet was employed. Use of saturated steam-water densities at 400°F gives a density difference of .369 psi/foot which translates, for 100-foot layer thickness, to a pseudo capillary pressure equalling 18.45 psi at $S_w = S_{wc} = .2$ and -18.45 at $S_w = 1.0$.

A number of 10,000-day model runs were performed for different well completion intervals. We assumed a tubing/casing configuration so that an additional variable was the layer in which the tubing bottom or withdrawal point was located. For example, with all layers 1-5 perforated, the tubing bottom could be placed in any one of the layers. A packer was assumed placed at top of formation.

A well target rate of 300,000 lbs/hour was specified for all runs with a minimum flowing wellbore pressure at tubing bottom of 160 psia. For all runs, time step was specified as 500 days. Table 3 summarizes model results at 10,000 days. The listed mass fraction produced, producing bottomhole quality, producing rate and produced Btu/lb all apply at the 10,000-day point in time. Average Btu/lb produced is cumulative energy produced over 10,000 days divided by cumulative mass produced. Energy produced is enthalpy, defined as $U + pv$ at producing cell conditions. Internal energy U is relative to a zero value for U of saturated water at 60°F.

Table 3 shows that the location of a single-layer (100 feet) completion is very important. Comparing runs 1-3 shows that cumulative mass fraction recovered at 10,000 days varies from 11.7% to 47.4% as a 100-foot producing interval is lowered from the top 100 feet to the bottom 100 feet of the 500-foot formation.

Runs 4-11 in Table 3 indicate that the perforated or open interval location is important while the location of the tubing bottom or withdrawal point within a given open interval is relatively unimportant. For example, Runs 4 and 5 show about equal recovery values for their top 300 feet open interval regardless of whether the tubing withdrew from the top 100 feet or bottom 100 feet of the interval. Runs 6-7 show the same result for a bottom 300-foot open interval regardless of the tubing position within the open interval. The best recoveries occur for a completely penetrated or open formation -- Runs 9-11 -- and performance is nearly independent of whether the tubing is set at top or bottom of the formation.

In Runs 1-5 the well was on deliverability in the first 500-day time step. Runs 6-7 and 9-11 produced the target 300,000 lbs/hour rate for 1,500 days and Run 8 produced the target rate for 500 days.

Taken together, Runs 1-11 indicate that a partial completion interval effectively drains the portion of the reservoir formation opposite and above the interval, but inefficiently drains the formation below it.

Spatial truncation errors in the results of Table 3 are very small as indicated by several runs we made using a 10 x 10 grid with ten 50-foot thick layers. Time truncation error was examined by repeating Run No. 10 using time steps of 250, 1,000, 2,000 and 5,000 days. Figure 3 shows producing rate and bottomhole producing quality vs. time calculated using the various time steps. The results with $\Delta t = 250$ and $\Delta t = 500$ days are virtually identical. The error with $\Delta t = 1,000$ days is significant but not large while $\Delta t = 2,000$ days causes an error bordering on acceptability. The surprising feature of these results is the small time truncation error for steps of 1,000 days or less in light of the large changes in saturation which occur in a single step.

The saturation changes stably computed in a single step are illustrated in Table 4 which shows saturations and pressures at the end of the first 2,000-day time step (all layers open, tubing at layer 3). Maximum saturation change was .9989 in grid block ($i=1, k=1$) and maximum pressure change was -441.4 psi in grid block ($i=1, k=5$). Initial pressures ranged from 469 to 618 psia from formation top to bottom, some 200 to 350 psi above saturation pressure corresponding to 400°F. That is, the model in this single step proceeded from a highly undersaturated, 100% liquid configuration to that shown in Table 4. Note, also, from Figure 3 that time truncation error for this first time step is virtually negligible. The reader should recall in viewing Table 4 that the first column of cells is the wellbore.

The calculated producing rate for this first 2,000-day step was 286,400 lbs/hour and bottomhole quality was .05794. Using Equation (33), the throughput ratio for withdrawal cell ($i=1, k=3$) was

$$R_T = 1.22(286,400)(2.8(.05794) + .018)(2,000) = 126 \times 10^6$$

This throughput ratio was achieved with the producing cell steam saturation changing from 0 to .8993. That is, it is not a throughput ratio corresponding to stabilized conditions

with small changes per time step. This ratio is three to four orders of magnitude larger than the 20,000 ratios we have previously achieved with semi-implicit models under high rate-of-change conditions.

Table 5 shows the number of required iterations per time step for each step for the three runs using $\Delta t = 500, 1,000$ and $2,000$ days. The numbers in parentheses in Table 5 are the maximum grid block saturation changes over the grid during each time step.

Table 6 shows calculated pressures and saturations after the first 500-day time step of Run No. 8. Producing rate and quality were 300,000 lbs/hour and .04, respectively, so that the throughput ratio from Equation (33) was

$$R_T = 1.22(300,000)(2.8(.04) + .018)(500) = 23.8 \times 10^6$$

This ratio was achieved with a high steam saturation change in the producing cell from 0 to .8481. Required iterations for this first step were 30. The iterations declined to 24 when initial pressure at formation top was reduced to 270 rather than 450 psia. The throughput ratio at 10,000 days for this run was 11.5×10^6 corresponding to a producing rate and quality of 53,100 lbs/hour and 1208, respectively.

Run 12 in Table 3 is identical to Run 10, except that permeability is 500 md rather than 100 md. The higher permeability resulted in a greater recovery of .7459 compared to .5656 at 10,000 days and gave a considerably higher producing quality of 7058 at 10,000 days. Run 12 produced the target 300,000 lbs/hour rate until 5,000 days. Figure 4 shows the effect of permeability on producing rate and quality vs. mass fraction produced. Producing quality in Figure 4 is calculated at a separator condition of 100 psia. The curves of average reservoir pressure (volumetrically weighted average of all grid blocks) vs. mass fraction produced are not plotted, but are identical for the two runs. Figure 4 shows that produced stream quality at the fixed separator condition is nearly a single-valued function of mass fraction produced and independent of permeability level.

Figure 5 shows average reservoir pressure vs. mass fraction produced calculated for 10,000-day runs using $k = 100$ and 500 and $\phi = .05$ and .35. The figure indicates that permeability level has a negligible effect on average pressure vs. mass fraction produced. The large porosity results in a very slightly lower average reservoir pressure. The small effect is due to the lower

rock heat capacity (i.e. less rock) in a higher porosity formation. This small effect of porosity on pressure decline is in contradiction to results reported elsewhere [4].

The average computer time per run for Runs 1-11 was 16 CDC 6600 CPU seconds. For the 10x5 grid and 20 steps per run this translates to .016 seconds per grid block-time step. This figure compares to a rough value of .01 seconds* per grid block-time step for our semi-implicit models.

SIMULATION OF A FRACTURED-MATRIX RESERVOIR

Many geothermal reservoirs are known or believed to be fractured-matrix systems. Conventional simulation is often used where extensive fractures are known to exist. Such simulation employs an assumption that flow in the matrix-fissure system can be adequately modeled by assuming an unfractured matrix formation with a high effective permeability reflecting the fracture system conductivity.

Here we examine the difference in simulated performances of a fractured reservoir sector modelled first as an unfractured formation, and second as a matrix-fissure system. While nature seldom provides near-uniformity in spacing of fractures, we must employ some semblance of uniform spacing to perform any calculations. We consider a fractured system consisting on the average of 40x40x40 feet matrix blocks separated by a three-dimensional orthogonal planar system of vertical and horizontal fractures.

To reduce the dimensionality of the matrix calculation, we treat the matrix cubes as cylinders of equivalent radius 22.5676 feet ($\pi r^2 = 40 \times 40$) and height of 40 feet. We have used this cylindrical approximation for several years in black oil fractured matrix simulation; it is partially justified since the physically real irregularity of fracture spacing and angles undoubtedly yields a variety of matrix block shapes deviating considerably from rectangular parallelepipeds.

Use of a fracture volume equal to 1% of combined fracture plus matrix volume leads to a fracture width of .029 feet. This figure assumes equal widths of horizontal and vertical fractures. From Muskat [10], fracture permeability for width w in cm, is

*This number can vary considerably. For "easy" multiphase flow problems (we omit definitions of "easy" for brevity), we have achieved times as low as .0018 seconds per block-step.

$$k = 10^8 w^2 / 12 = 6.5 \times 10^6 \text{ Darcies} \quad (34)$$

for the .029 feet width. In simulating flow in fracture grid blocks, it is only necessary to use fracture permeabilities large enough to render viscous forces negligible in comparison with gravitational forces. In previous black oil fractured matrix reservoir work and in this work, we have found results insensitive to use of fracture permeabilities higher than 10 to 20 Darcies.

For the purpose of computations described here, the fracture system conductivity is assumed sufficiently large that the reservoir behavior is dominated by vertical transients in pressure, temperature and saturation. The fracture conductivity is assumed sufficient to maintain negligible areal gradients of these quantities. For example, by this assumption any steam-water contact in the fractures will be nearly horizontal over a wide areal expanse.

The withdrawal rate used for computations was based on a well spacing of about 300 acres with rates of 300,000 lbs H₂O/hour per well. This translates to a rate of about 40 lbs/hour for a 1,240-foot vertical column section of the reservoir with areal dimensions 40x40 feet. The vertical gridding consisted of six matrix blocks each subdivided vertically into 10-foot grid blocks and one last deep 1,000-foot matrix grid block. Calculations were terminated before steam-water contacts reached the deep block so that its lack of gridding is immaterial.

In the matrix-fissure simulation, the vertical and horizontal fractures were included in the grid system. Vertically, then, six additional grid blocks each .029 feet thick separated the six matrix blocks and the total number of vertical blocks was $6 \times 4 + 6 + 1$ or 31. We obtained nearly identical results using three and two grid blocks radially for the matrix-fissure system. Results given here are for the case of two radial grid blocks. The first radial block was matrix with an inner boundary radius of 0, an outer boundary radius of 22.5676 feet and a "center" radius equal to the volume mean value of 15.96 feet. The second radial grid block was vertical fracture with inner radius of 22.5676 feet and outer radius of $22.5676 + .029/2$ feet. Figure 6 illustrates this radial-z grid for the fissure-matrix simulation. Fluid was withdrawn from the bottom 1,000-foot thick vertical fracture block.

Matrix permeability and porosity were 1 md and 0.2, respectively. Grid block pore volumes for the matrix-fissure system illustrated in Figure 6 were

Grid Block	Pore Volume, Res. Bbls.
10-foot matrix	569.9
.029-foot horizontal fracture radial block #1	8.26
.029 x .0145-foot fracture intersection block	.0106
10-foot vertical fracture	3.66

Initial reservoir pressure was 270 psia at top of formation and temperature was 400°F. Overburden heat loss (gain) had a small effect and was ignored. Heat conduction in the matrix was modeled using a thermal conductivity of 38 Btu/ft-day-°F. Matrix rock heat capacity was 35 Btu/cu.ft. rock-°F. Relative permeabilities of Equations (26) and a linear rock capillary pressure curve of $P_c = 0$ at $S_w = 1$, $P_c = 10$ psi at $S_w = 0$ were used for matrix and zero capillary pressure and linear $k_r = S$ curves were used for the fractures.

The 2 x 31 (radial-z) matrix-fissure simulation was run to 1,500 days for a rate of 40 lbs/hour and to 4,200 days for a rate of 10 lbs/hour. Two runs were made for the 40 lbs/hour rate, the first with a constant 30-day time step, the second with a constant 60-day time step.

Figure 7 shows calculated water saturation vs. depth from top of formation at 1,500 days for the 40 lbs/hour production rate. The solid lines correspond to the 30-day time step while the circles and dashed line show results for the 60-day step. The vertical tic marks indicate water saturations in the first radial horizontal fracture blocks.

This figure shows the poor recovery of water from the matrix blocks due to the capillary discontinuities imposed by the horizontal fractures. Each matrix block above the (vertical fracture) steam-water contact transiently drains toward an equilibrium final saturation vs. depth distribution determined by the rock capillary pressure curve and the zero P_c condition at each matrix block bottom imposed by the horizontal fracture. The significant transient effect is indicated by the decrease in water recovery with matrix block depth. This is due, of course, to the longer times of drainage experienced by higher located matrix blocks.

The horizontal fracture blocks opposite the 100% steam saturated vertical fracture grid blocks rapidly rise toward 100% steam saturation. Above the steam-water contact, the water draining from the bottom of a matrix block enters the horizontal fracture block and then preferentially flows vertically down into the top of the next lower matrix block rather than laterally into the vertical fracture. This preference is very close to 100%. These latter results are shown by model printouts of water and steam interblock flow rate magnitudes and directions at selected times.

Table 7 summarizes average iterations per time step, average saturation change (maximum over grid) per time step and computing times for the three fractured-matrix simulation runs. The negligible time truncation error for 30- and 60-day time steps shown in Figure 7 is somewhat surprising in light of the average saturation change rising from .38 for the 30-day step to .66 for the 60-day step. The .66 figure is actually conservative since 27 vertical fracture grid blocks were swept from 0 to 100% steam saturation in only 25 steps in Run 2. No time steps were repeated due to divergence in any of these runs in spite of nearly 100% saturation changes in one step for the .01 RB pore volume fracture-intersection grid blocks. Both Runs 1 and 2 experienced a number of time steps of 90-100% saturation change. Run No. 1 computing time corresponds to a time per block-step of about .01 seconds.

Figure 8 compares the effect of producing rate on matrix-fissure simulation results. The calculated saturations for Run 1 at 40 lbs/hour and Run 3 at 10 lbs/hour are compared at times of equal cumulative production. The steam-water contact for the higher rate is 40% (140 feet vs. 101 feet) deeper due to the shorter time available for transient water drainage from the matrix blocks above the contact.

Conventional simulation results were generated by running the model in one-dimensional vertical mode using 24 10-foot blocks and one 1,000-foot block. The dashed line in Figure 9 shows resulting calculated water saturation vs. depth at 1,500 days for an "effective" permeability of 50 md and a producing rate of 40 lbs/hour. Gravity forces dominate and the conventional results show a sharp transition zone from a drained ($S_w = S_{wc} = .2$) upper region to the 100% water zone. The transition zone is considerably higher than the matrix-fissure simulation results viewing either the matrix or the vertical fracture steam-water contact.

We can achieve somewhat greater realism in the conventional simulation by utilizing the fact that the capillary discontinuities each 40 feet impose a maximum final recovery of water (by flow alone) which can be pre-determined using the rock capillary pressure curve, the 40-foot matrix block height and the .369 psi/foot water-steam density (gradient) difference. Following Reference [8] we integrate the $S_w - P_c$ relation over the 40 feet using the fact that $P_c = 0$ at matrix block bottom and find that final minimum average matrix block water saturation is .417. Using this value for S_{wc} in the relative permeability equations, the conventional simulation gives the water saturation profile indicated by the larger dashed line in Figure 9.

Further adjustments in various data might be made to narrow the difference between matrix-fissure and conventional simulation results. Considering the basic difference in mechanisms for the conventional and more correct matrix-fissure calculations, we hold little hope for forcing accuracy from a conventional simulation. In particular, the above described rate effect (Figure 8) is shown by the more rigorous matrix-fissure simulation, but not by conventional simulation (unless the permeability used is very low).

A full three-dimensional simulation of a fractured-matrix reservoir will require tying in this vertical two-dimensional R-Z matrix-fissure calculation to a two-dimensional areal calculation where the areal blocks communicate through the fracture system and the interblock flows reflect the different "sector" or areal block steam-water contacts. This task will involve a significant effort in logic and coding and will in many cases require disk on fixed memory machines. The two-dimensional R-Z matrix-fissure calculation described here is adequate only if the areal gradients within the reservoir are assumed small due to high fracture conductivity.

Interpretation of Pressure Drawdown Tests

The major differences between conventional and matrix-fissure simulation results just described arose because of the two-phase flow in a system having capillary discontinuities. Here we illustrate difficulties which can arise in using conventional simulation to interpret pressure drawdown tests in fractured-matrix, hot water systems with single-phase water flow.

Simulation of a well test in a system having a three-dimensional network of orthogonal fracture planes would require a full three-dimensional Cartesian grid. To simplify for the purpose of illustration, we consider a system of 44-foot matrix layers separated by horizontal fractures. A 10x5 radial-z grid was used to model a horizontal disk of matrix beneath a horizontal fracture. The disk dimensions were exterior radius $r_e = 10,000$ feet and thickness = 22 feet. The five layer thicknesses were $w/2, 2, 4, 8, 8$ feet where w is horizontal fracture thickness. This disk is a symmetrical element for the case where the well penetrates the entire formation thickness.

The radial spacing was calculated using Equation (29) with the wellbore included in the grid. Wellbore radius was .25 and the 10 block "center" radii were .25, .43, 1.38, 4.48, 14.55, . . . , 5,242.37 feet. Pore volumes of the wellbore cells varied from .000014 to .2798 RB in layers 1-5 for a small fracture width $w = .245$ mm.

Matrix and fracture layer porosities were .2 and 1.0, respectively. Initial temperature was uniformly 350°F and initial pressure was 2800 psia at top of formation. The illustrative pressure drawdown test consisted of producing 10,000 lbs/hour from a well open in all five layers for ten days. Fracture conductivity and matrix permeability were varied in five simulation runs as tabulated in Figure 10. The fracture permeabilities were related to fracture width by the relationship $k = 10^8 w^2 / 12$ where k is in Darcies and w in cm. The homogeneous (no fracture) case, Run 4, has a permeability of 90.9 md, which gives a total md-ft product for the 22-foot thickness equal to that of the fracture cases.

Figure 10 shows calculated pressure drawdown (initial pressure-flowing wellbore pressure) vs. time on a semi-log plot for five cases. The homogeneous case (Run 4) gives a straight-line and use of the well-known relationship, slope = $Q\mu/4\pi kh$, gives $k = 90.9$ md, in agreement with the value used. Arbitrary use of the average slope from .1 to 1 days with the relation slope = $Q\mu/4\pi kh$ gives $k = 247, 188$ and 157 md for Runs 1-3, respectively. These permeabilities bear little resemblance to either fracture or matrix permeabilities.

The semi-log plots of pressure drawdown vs. time actually are not linear for the fracture cases, but are rather concave upward. This results from the fact that the reservoir transient is primarily a crossflow (vertical) bleeding of fluid into the fracture rather than the radial transient of a homogeneous unfractured formation. The degree of upward curvature of the drawdown curve increases as matrix permeability decreases.

The cases of small fracture width, Runs 1-3, exhibit a rapid initial drawdown of 60-80 psia in the first few minutes of flow. The calculated effect of a fivefold larger fracture width is one of reducing this early drawdown to 2-3 psi. However, for times after the first few minutes, the larger fracture gives a calculated, concave upward drawdown curve of shape virtually identical to that for the smaller fracture. This is illustrated by the curves for Runs 1 and 5 in Figure 10.

Figure 11 shows calculated drawdowns for a tenfold larger horizontal fracture spacing of 440 feet. The simulations used a 10 x 8 grid with the eight layer thicknesses equal to .0004, 2, 4, 8, 16, 32, 64 and 94 feet (a total thickness of 220 feet). The k_w product for the total fracture width of .0008 feet (.245 mm) is 4 Darcy-feet. A drawdown test flow rate of 100,000 lbs/hour was specified. The curve for this Run 6 in Figure 11 shows a linearity of drawdown vs. $\ln(t)$ past 10 days to about 30 days. The upward concave curve shape from 100 to 1,000 days is due to establishment of semi-steady-state conditions throughout the reservoir.

The curve labeled Run 7 in Figure 11 was calculated for a 220-foot homogeneous reservoir with $k = 9.09$ md corresponding to an equivalent total md-feet product of 2,000. The slopes of the curves for Runs 6 and 7 on Figure 11 give formation permeabilities of 18 md and 9.09 md, respectively. If the 10-day test portion of the Run 6 curve were analyzed by conventional radial flow theory, then a permeability of 18 md and a skin factor of 9.65 would be determined. The circles of Run 8 in Figure 11 show the simulator results for a homogeneous reservoir with this permeability and skin factor. Figure 11 shows that calculated drawdowns for the fractured formation (Run 6) and for an 18 md, homogeneous formation with skin (Run 8) agree well through 1,000 days.

These results of Figure 11 indicate that for the particular fracture spacing and width of 440 feet and .245 mm, respectively, conventional radial flow analysis would (a) yield erroneous permeability and skin but (b) give accurate long-term deliverability predictions. This conclusion does not hold for the previously discussed results of Figure 10 corresponding to the smaller fracture spacing of 44 feet. For this spacing, the short-term drawdown test can fail to yield any linearity from which conventional analysis can determine effective permeability and skin.

Several additional complexities that may exist in practice need mentioning in connection with the results just discussed. A naturally fractured formation will generally have vertical as well as horizontal fractures. Accounting for a three-dimensional network of fracture planes with the model

described herein would require a three-dimensional simulation. If fracture spacing were the order of 100 feet or less, a very large number of grid blocks would be required. A better modelling approach in this case would be a dual porosity formulation where interblock flow is assumed to occur only in the fracture system. The matrix would be accounted for by zero-dimensional, one-dimensional spherical or two-dimensional cylindrical subcalculations tied into the fracture porosity in each grid block. The heat-loss calculation described in Reference [3] is an example of this type of formulation.

The model described here may apply well to an artificially fractured formation since in this case the vertical fractures will intersect the well. An $r-\theta-z$ grid representing a symmetrical element in this case may accurately model well performance with a reasonably low number of grid blocks.

An upward concave deviation from linearity in a drawdown test curve may result from factors other than formation fractures. Geothermal reservoirs with brines of high salinity may precipitate salt with pressure drawdown near the well. This can cause a skin factor increasing with time and the mentioned deviation from linearity. It is well-known that faults or other flow barriers near a well can cause upward curvature. Short-term drawdown tests on wells which partially penetrate thick formations, especially where the ratio of vertical to horizontal permeability is small, can result in deviation from linearity. Regardless of penetration, a formation consisting of alternating tight and permeable streaks of large permeability contrast can yield deviation from linearity through the same vertical, crossflow type of transient treated above in the horizontally fractured formation calculations. Quoting from Reference [11], which treated simulation of single-phase gas flow, ". . . The reservoir picture finally employed with success stemmed from the hypothesis that the well communicated with a number of thin permeable stringers . . . fed by severely limited crossflow from large sand volumes. . .". In that work, for such reservoirs, the calculated and observed drawdown/buildup curves failed to yield the linearity of conventional analysis.

Finally, the fractured formation, drawdown test illustrative calculations and interpretations presented here are not unique to geothermal reservoirs, but apply to any formation subject to single-phase flow of a low compressibility fluid -- oil, water or high pressure gas.

HEAT EXTRACTION FROM HOT DRY ROCK

We consider a vertical fracture in a hot dry rock initially at 500°F. A 5x5x5 three-dimensional grid describes a rectangular parallelepiped with $\Delta x = \Delta z = 80$ feet and $\Delta y = .01, 30, 120, 160, 320$. These dimensions resulted from combining blocks in a comparison run which used y-direction increments of .01, 10, 20, 40, 80, 160 and 320 feet. The overall dimensions are a 400x400-foot vertical crack of .02-foot width with 630 feet of rock either side of it. The 630 feet of rock in the y-direction is sufficiently large that the system acts as infinite for the 3,000 days of simulation. Different grids were used to determine the acceptably low spatial truncation error of the 5x5x5 grid.

Since the system is symmetrical about the vertical midplane of the crack, this 5x5x5 grid represents half the system. Crack width is of no consequence except in its relation to the kw product where k is fracture permeability and w is fracture total width. In the grid plane $j = 1$ (the crack) an $x-z$ thermal conductivity of 3.8 Btu/ft-day-°F was used, porosity was 1.0 and permeability was varied over a number of runs from 10 Darcies to 800,000 Darcies. In the planes, $j = 2-5$ (hard rock) thermal conductivity was 38 Btu/ft-day-°F, rock specific heat was 35 Btu/cu.ft.rock-°F and porosity and permeability were zero.

100°F cold water injection rate was specified as 25,000 lbs/hour into the bottom left corner of the crack (cell $i=1, j=1, k=5$). A withdrawal well at the upper right corner of the crack (cell $i=5, j=1, k=1$) maintained pressure at 800 psia due to a large specified productivity index. This withdrawal well produced on deliverability against the 800 psia pressure. The 25,000 lbs/hour injection rate corresponds to actual injection well rate of 50,000 lbs/hour since the grid represents a symmetrical half of the total system.

Figure 12 shows calculated energy recovery and producing well bottomhole temperature vs. time. Energy recovery is defined as cumulative enthalpy produced divided by the sensible heat above 100°F initially contained in a portion of the rock. The portion used is the first 310 feet since the last 320 feet experienced essentially no recovery (temperature decline) at 3,000 days. The initial energy in place on these bases is 6.944×10^{11} Btu. Enthalpy of produced water is $U + pv$ where internal energy U is zero at 100°F.

Figure 12 shows a rapid decline of produced water temperature from 500°F to less than 300°F in the first few days followed by a very flat decline from 170°F to 137°F from 1,000 to 3,000 days. Fractional energy recovery is 0.1663 at 3,000 days, equivalent to 1.155×10^{11} Btu or an average of 64 Btu/lb water produced (enthalpy relative to zero U at 100°F). The average temperature corresponding to this average enthalpy is about 162°F.

The fracture width w controls system conductivity or throughput. The corresponding parameter or group of importance is the kw Darcy-foot product, which is proportional to w^3 since fracture permeability is proportional to w^2 . We used permeabilities up to 800,000 Darcies with the .02-foot model dimension for the fracture. This 16,000 Darcy-foot kw product corresponds to a fracture width of 4 mm using the fracture permeability equation $k = 10^8 w^2 / 12$ (w in cm). Fracture width, i.e. the kw product, had no effect on the calculated recovery and temperature shown in Figure 12.

Model runs were made with the injection well located higher, 200 feet from top of formation in cell $i=1, j=1, k=3$. The change of injection location had no effect on calculated recovery and producing temperature.

Figure 12 also shows calculated recovery and temperature for a larger fracture of dimension 800x800 feet. Again, the above described kw product and injection well location variations had no effect on the calculated recovery and producing temperature. The larger fracture resulted in a considerably higher bottomhole producing temperature vs. time and a lower fractional energy recovery. Calculated absolute energy recovery at 3,000 days was higher for the larger fracture -- 3.53×10^{11} Btu vs. 1.155×10^{11} Btu for the 400x400 foot fracture. Thus, a fourfold increase in fracture area caused a threefold increase in energy recovery. Average enthalpy of produced water was 196 Btu/lb corresponding to an average temperature of produced water of 292°F.

The runs were performed using automatic time step control due to the rapid initial transients. With a first time step of .1 days, a subsequent minimum Δt of .2 days, control by 150°F maximum grid block temperature change per time step and a maximum time step of 500 days, the model took 13 time steps to 3,000 days for the 100,000 Darcy permeability. Computer time for this run was 46 CDC 6600 CPU seconds. Twenty of these seconds were required for the first two time steps.

Calculated results for permeabilities less than 100,000 Darcies exhibited no circulatory "free" convection type cells in the vertical fracture plane. Table 8 shows an example of these results at 3,000 days for the case of a 400x400 foot fracture, and 100,000 Darcies fracture permeability which corresponds to a 2 mm fracture width. The table shows calculated pressures in the fracture plane, temperatures in all planes and interblock flow rates (positive to the right and vertically downward). Water flow is uniformly to the right and upwards away from the injection in grid cell $i=1, j=1, k=5$. Temperature uniformly increases to the right and upward (in the directions of water flow) except in the top row.

Results for the 800,000 Darcy permeability differed markedly from those just described. Table 9 shows pressure, temperature and flow rate distributions at 75 days for the 800x800 foot fracture with 800,000 Darcies. y -direction spacing was altered in this run to .01, 10, 30, 90, 180 feet. The flow rates in Table 9 show extremely strong "free" convection cells in the 5x5 grid of the vertical fracture plane. Water is in fact flowing downward into the injecting cell $i=1, j=1, k=5$. The flow distribution is complex and the temperature change from left to right alternates in sign in alternate rows corresponding to alternation in direction of horizontal flow rate.

Table 10 shows pressure, temperature and flow rate distributions for this 800,000 Darcy case at 3,000 days. While the flow rates are much more uniform with flow uniformly upward, the free convection still exists with some horizontal flow from right to left. Deviations from a pattern of uniform temperature increase to the right and upward are small but exist and are complex. This 800,000 Darcy run was much more difficult than the runs for 100,000 or fewer Darcies. The number of time steps increased to 21 and computer time increased to 144 CDC 6600 CPU seconds, largely due to divergence and repeat of one of the time steps.

These fractured hot rock simulations did not employ any enhanced heat conduction to the fracture due to thermal cracking induced by temperature decrease. A functional relationship between thermal conductivity and temperature or temperature change can be included in the model. Such a relationship and associated parameters might be deduced from laboratory or field experimental data.

SUMMARY

An implicit, three-dimensional geothermal model is described and partially evaluated in respect to stability or time step tolerance. The model is only partly implicit in certain applications where various terms associated with allocation of well rates among open layers are treated explicitly.

The implicit model stably accommodated time steps corresponding to 80-100% saturation change in a grid block and throughput ratios the order of 10^8 in several illustrative multiphase flow problems. This compares with our experience of limits of 3-10% saturation change and throughput ratio of roughly 20,000 with semi-implicit geothermal and oil reservoir models. The implicit model stability allowed inclusion of fractures and wellbores as small-volume grid blocks in several multiphase flow test problems.

An analytical derivation is presented for a well deliverability reduction factor which can be used in simulations using large grid blocks. The factor accounts for increased pressure drop near the well due to hot water flashing and steam expansion.

The model was used to simulate two-phase depletion of a fractured matrix reservoir with horizontal and vertical fractures included as grid blocks. The results were poorly matched by conventional simulation which treats the reservoir as an unfractured formation with high effective permeability.

Simulation of a single-phase flow, pressure drawdown test in a tight formation with horizontal fractures showed upward concave curvature of the pressure drawdown vs. $\ln(t)$ plot. The degree of calculated curvature and attendant interpretation difficulty increased with decreasing matrix permeability level and decreasing horizontal fracture spacing.

The final illustrative application treated heat extraction from a fractured, hot dry rock system. For a given cold water injection rate, the calculated energy recovery and production well water temperature vs. time were not affected by fracture permeability-width product or injection well location. The fracture conductance was varied from 2 to 16,000 Darcy-ft, while injection well location was varied only from the bottom corner to the mid-depth of the fracture plane. A fourfold increase in fracture area from 400x400 to 800x800 square feet resulted in a threefold increase in calculated energy recovery at 3,000 days for the same cold water injection rate.

A limited investigation of time truncation error indicates that acceptably low levels can occur in spite of average maximum (over grid) saturation changes per time step as high as 60%.

NOMENCLATURE

A	cross-sectional area normal to flow, ft^2
c	compressibility, 1/psi
C_p	specific heat, Btu/lb-°F
$(\rho C_p)_R$	rock specific heat, Btu/cu.ft rock-°F
f_w	water phase volumetric fractional flow
f_g	gas phase volumetric fractional flow
f	well deliverability factor, fraction
H	enthalpy, $U + pv$, Btu/lb
k	absolute permeability, md
k_r	relative permeability, fraction
k_{rgcw}	relative permeability to gas at irreducible water saturation S_{wc}
K	thermal conductivity, Btu/ft-day-°F
N_x, N_y, N_z	numbers of grid blocks in reservoir grid system, in x, y, z directions, respectively
\bar{q}	desired or target production rate, lbs $\text{H}_2\text{O}/\text{day}$
q	production rate, lbs $\text{H}_2\text{O}/\text{day}$
q_H	enthalpy production rate, Btu/day
q_{HL}	heat loss rate, Btu/day
$p_s(T)$	water vapor pressure
p	gas phase pressure, psia
p_{wb}	wellbore flowing pressure, psia
p_c	capillary pressure, $p_g - p_w$, psi
R_T	throughput ratio, Equation (31)
r	radius, feet

r_e	exterior radius
r_w	wellbore radius
RB	Reservoir Barrels
S	skin factor
S_w	water phase saturation, fraction
S_g	gas phase saturation, fraction
S_{ge}	gas saturation at $r = r_e$
S_{wc}	irreducible water saturation
S_{gc}	critical gas saturation
t	time, days
Δt	time step, $t_{n+1} - t_n$, days
T	temperature, °F
T_s	water saturation temperature, $T_s(p)$, °F
U	internal energy, Btu/lb
V_p	grid block pore volume, $V\phi$
V	grid block bulk volume, $\Delta x\Delta y\Delta z$, cubic feet
v	specific volume, cu.ft/lb
w	fraction width
X	quality, mass fraction steam
x,y,z	Cartesian coordinates, feet, z measured positively vertically downward
$\Delta x, \Delta y, \Delta z$	grid block dimensions, feet

GREEK

$\bar{\delta}$	time difference operator, $\bar{\delta}X \equiv X_{n+1} - X_n$
δ	iteration difference operator, $\delta X \equiv X^{\ell+1} - X^\ell$
ϕ	porosity, fraction
ρ	density, lbs/cu.ft
γ	specific weight or gradient, psi/ft ($\gamma_w = \rho_w/144$)
λ	mobility, k_r/μ

T_c	reservoir heat conduction transmissibility KA/ℓ , where ℓ = distance between grid block centers, Btu/day-°F
T_g	gas phase transmissibility, $(kA/\ell)(k_{rg}^o/\mu_g) \times .00633$, lbs gas phase/day-psi
T_w	water phase transmissibility, $(kA/\ell)(k_{rw}^o/\mu_w) \times .00633$, lbs water phase/day-psi
$\Delta(T\Delta P)$	$= \Delta_x(T_x\Delta_x P) + \Delta_y(T_y\Delta_y P) + \Delta_z(T_z\Delta_z P)$, defined as indicated above Equation (5)
μ	viscosity, cp

SUBSCRIPTS

e	exterior
g	gas (steam) phase
i,j,k	grid block indices, x_i, y_j, z_k
k	grid layer number or index
ℓ	(superscript) iteration number
n	time level, t_n
s	saturation condition
x,y,z	denotes x, y or z direction, respectively
w	water phase
wb	wellbore

REFERENCES

- Coats, K. H., and Ramesh, A. B., "Numerical Modeling of Thermal Reservoir Behavior", Preprint presented at the 28th Annual Technical Meeting of the Petroleum Society of C.I.M., Edmonton, Alberta, May 27-June 6, 1977.
- Carter, R. D., and Tracy, G. W., "An Improved Method for Calculating Water Influx", Trans. AIME (1960), 219, 415-417.
- Coats, K. H., George, W. D., Chu, Chieh, and Marcum, B. E., "Three-Dimensional Simulation of Steamflood-ing", Trans. AIME (1974), 257, 573.

4. Toronyi, R. M., and Ali, S. M. Farouq, "Two-Phase, Two-Dimensional Simulation of a Geothermal Reservoir", Soc. Pet. Eng. J. (June, 1977), 171-183.
5. Blair, P. M., and Weinaug, C. F., "Solution of Two-Phase Flow Problems Using Implicit Difference Equations", Trans. AIME (1969), 246, 417.
6. Price, H. S., and Coats, K. H., "Direct Method in Reservoir Simulation", Trans. AIME (1974), 257, 295.
7. Steam Tables, Keenan, J. H., and Keyes, F. G., Hill, P. G., and Moore, J. G., John Wiley & Sons, 1969.
8. Coats, K. H., Nielsen, R. L., Terhune, M. H., and Weber, A. G., "Simulation of Three-Dimensional Two-Phase Flow in Oil and Gas Reservoirs", Soc. Pet. Eng. J. (December, 1967), 377-388.
9. Coats, K. H., Dempsey, J. R., and Henderson, J. H., "The Use of Vertical Equilibrium in Two-Dimensional Simulation of Three-Dimensional Reservoir Performance", Trans. AIME (1971), 251, 63-71.
10. Flow of Homogeneous Fluids, Muskat, M., J. W. Edwards, Ann Arbor, Michigan, 1946.
11. Coats, K. H., Dempsey, J. R., Ancell, K. L., and Gibbs, D. E., "Analysis and Prediction of Gas Well Performance", SPE 3474 presented at 46th Annual Meeting of SPE, New Orleans, Louisiana, October 3-6, 1971.

APPENDIX

CALCULATION OF DELIVERABILITY FACTOR f

We consider two-phase, steady-state steam-water flow from some exterior radius R to wellbore radius r_w . The point R is assumed to be saturated, and pressure is P at R and p_{wb} at r_w .

Darcy's law gives liquid water phase flow rate at any radius as

$$q_w = q(1 - X) = -2\pi k\Delta z \lambda_w \rho_w r dp/dr \quad (35)$$

where X is flowing steam quality, q is total flow rate, lbs H₂O/day, $k\Delta z$ is md-ft product $\times .00633$, λ_w is k_{rw}/μ_w and ρ_w is water density in lbs/cu.ft. Integration using the fact that q is constant gives

$$q = \frac{2\pi k\Delta z}{\ln \frac{R}{r_w}} \int_{p_{wb}}^P \frac{\lambda_w \rho_w}{1-X} dp \quad (36)$$

or

$$q = \frac{2\pi k\Delta z}{\ln \frac{R}{r_w}} I(P, p_{wb}, S_g) \quad (37)$$

where the integral I is a function only of the integration limits p_{wb}, P and of steam saturation S_g at R because, as we will now show, the integrand $\lambda_w \rho_w / (1-X)$ is a single-valued calculable function of pressure p.

Flowing quality X is related to fractional flow by

$$X = 1 / (1 + f_w \rho_w / (1 - f_w) \rho_g) \quad (38)$$

and enthalpy per lb of flowing stream is

$$H = XH_g + (1 - X)H_w \quad (39)$$

At steady-state, flowing stream enthalpy is constant and from (39),

$$X = (H - H_w) / (H_g - H_w) = X(p), \quad (40)$$

where the dependence upon pressure alone follows from the fact that H is constant and saturated water and steam enthalpies are single-valued functions of pressure. From Equation (39),

$$f_w = 1 / [1 + X \rho_w / (1 - X) \rho_g] = f_w(p) \quad (41)$$

where the dependence upon pressure alone follows from the fact that saturated water and steam densities are single-valued functions of pressure.

If p and S_g at R are given, then enthalpy H can be calculated from Equations (38) and (39). Given H, we can calculate the values of X(p) and $f_w(p)$ at any pressure from Equations (40) and (41). Thus, the integral in Equation (36) can be numerically integrated for any given values of P, p_{wb} and S_g .

We now consider a grid block of large dimensions, $\Delta x \approx \Delta y$, with equivalent exterior radius r_e determined by $\pi r_e^2 = \Delta x \Delta y$. Assuming steady-state single-phase water flow from an undersaturated condition at r_e to saturation point R , Darcy's law gives

$$q = \frac{2\pi k \Delta z}{r_e \ln \frac{r_e}{R}} (\lambda_{we} \rho_{we} + \lambda_{ge} \rho_{ge}) (p_e - P) \quad (42)$$

where P is pressure at saturation point radius R and λ_{ge} is zero if $R < r_e$. Equation (37) describes flow from saturation point R to r_w and can be written

$$q = \frac{2\pi k \Delta z}{\ln \frac{R}{r_w}} \frac{I(\lambda_{we} \rho_{we} + \lambda_{ge} \rho_{ge})}{(\lambda_{we} \rho_{we} + \lambda_{ge} \rho_{ge}) (P - p_{wb})} (P - p_{wb}) \quad (43)$$

Solving for $p_e - P$ from (42) and $P - p_{wb}$ from (43) and adding the results gives

$$q = \frac{2\pi k \Delta z (\lambda_{we} \rho_{we} + \lambda_{ge} \rho_{ge})}{\ln \frac{r_e}{R} + \frac{1}{f} \ln \frac{R}{r_w}} (p_e - p_{wb}) \quad (44)$$

where

$$f = \frac{I(P, p_{wb}, S_{ge})}{(\lambda_{we} \rho_{we} + \lambda_{ge} \rho_{ge}) (P - p_{wb})} \quad (45)$$

In Equations (44), (45), if the exterior radius r_e is undersaturated, $\lambda_{ge} = 0$ and R must be calculated by trial and error if p_e and p_{wb} are given. P is, of course, equal to saturation pressure corresponding to temperature at r_e . If q is given, then R can be calculated directly from (42).

If the exterior radius r_e is saturated, then $R = r_e$, $P = p_e$ and Equation (44) becomes

$$q = \frac{2\pi k \Delta z}{r_e \ln \frac{r_e}{r_w}} f (\lambda_{we} \rho_{we} + \lambda_{ge} \rho_{ge}) (p_e - p_w) \quad (46)$$

where f is given by (45) with $P = p_e$.

We have used an analysis similar to that given here to calculate reduced deliverability of oil wells due to release and expansion of solution gas accompanying pressure decline near the well.

TABLE 1
SINGLE-WELL RADIAL FLOW TEST PROBLEM

Formation Thickness	=	500 ft
Permeability	=	100 md
Porosity	=	0.2
Wellbore Radius	=	0.25 ft
Exterior Radius	=	2,000 ft
Initial Pressure at Formation Top	=	450 psia
Initial Temperature	=	400°F
Initial Saturation S_w	=	1.0
Capillary Pressure	=	0
k_{rw} , k_{rg} from Equations (26)		
Res. and Overburden K	=	38 Btu/ft-D-°F
Res. and Overburden C_p	=	35 Btu/cu.ft Rock-°F
Rock Compressibility	=	4×10^{-6} 1/psi
Minimum Wellbore Pressure	=	160 psia

BLOCK	WELLBORE NOT INCLUDED IN GRID		WELLBORE INCLUDED IN GRID		BLOCK PORE VOLUME RES. BBLS*
	GRID BLOCK RADIUS, FEET		GRID BLOCK RADIUS, FEET		
	CENTER	INNER BOUNDARY	CENTER	INNER BOUNDARY	
1	.4	.25	.25	0	3.50
2	1.07	.68	.40	.25	4.45
3	2.91	1.84	1.07	.68	3.28×10
4	7.91	5.00	2.91	1.84	2.42×10^2
5	21.46	13.57	7.91	5.00	1.78×10^3
6	58.25	36.84	21.46	13.57	1.31×10^4
7	158.10	100.00	58.25	36.84	9.67×10^4
8	429.16	271.44	158.10	100.00	7.13×10^5
9	1164.92	736.81	429.16	271.44	5.25×10^6
10	-	-	1164.92	736.81	3.87×10^7

*THESE PORE VOLUMES ARE FOR BLOCKS IN ONE 100-FOOT LAYER.

TABLE 2
EFFECT OF TIME STEP SIZE ON
ONE-DIMENSIONAL RADIAL FLOW RESULTS

	<u>TIME, DAYS</u>		<u>TIME STEP SIZE, DAYS</u>						
	<u>4000</u>		<u>250</u>	<u>500</u>	<u>1000</u>	<u>2000</u>	<u>4000</u>		
MASS FRACTION PRODUCED	.1670		.1669	.1669	.1665	.1642			
BOTTOMHOLE QUALITY	.0559		.0566	.0576	.0583	.0576			
RATE, 1000's LBS/HR	115.3		113.8	111.9	111.6	115.4			
	<u>8000</u>		<u>250</u>	<u>500</u>	<u>1000</u>	<u>2000</u>	<u>4000</u>	<u>8000</u>	
MASS FRACTION PRODUCED	.3150		.3133	.3102	.3048	.2950	.2756		
BOTTOMHOLE QUALITY	.0674		.0671	.0668	.0667	.0665	.0638		
RATE, 1000's LBS/HR	90.5		90.9	91.2	91.3	92	96.9		
	<u>16000</u>		<u>250</u>	<u>500</u>	<u>1000</u>	<u>2000</u>	<u>4000</u>	<u>8000</u>	<u>16000</u>
MASS FRACTION PRODUCED	.4959		.4935	.4889	.4803	.4644	.4357	.3865	
BOTTOMHOLE QUALITY	.1442		.1420	.1380	.1310	.1197	.1039	.0835	
RATE, 1000's LBS/HR	43.5		44	45	46.9	50.2	56.3	67.9	

TABLE 5

NUMBER OF ITERATIONS PER TIME STEP
ALL LAYERS OPEN; TUBING IN LAYER 3

	<u>At, DAYS</u>		
	<u>500</u>	<u>1000*</u>	<u>2000</u>
25 (.9164)		29 (.9891)	41 (.9989)
7 (.5446)		4 (.2000)	22 (.4297)
8 (.7186)		14 (.6517)	6 (.4101)
8 (.2142)		9 (.3229)	5 (.1813)
10 (.2012)		5 (.2239)	5 (.2205)
6 (.1571)		6 (.2273)	
5 (.1064)		4 (.1826)	
5 (.1329)		5 (.0948)	
9 (.1211)		4 (.1334)	
3 (.1200)		4 (.1176)	
4 (.1040)		2 (.0973)	
5 (.0645)			
6 (.0481)			
4 (.0589)			
4 (.0681)			
3 (.0672)			
3 (.0624)			
2 (.0591)			
2 (.0551)			
2 (.0529)			

*THE SECOND TIME STEP AUTOMATICALLY CUT TO 100 DAYS DUE TO DIVERGENCE; THE 11TH STEP WAS 900 DAYS; ALL OTHER STEPS WERE 1,000 DAYS.

TABLE 6

CALCULATED RESULTS AFTER FIRST 500-DAY TIME STEP
TWO-DIMENSIONAL RADIAL-Z RESULTS; LAYERS 2-4 OPEN; TUBING AT LAYER 3

<u>PRESSURE AT GRID BLOCK CENTER (psia)</u>										
	<u>1</u>	<u>2</u>	<u>3</u>	<u>4</u>	<u>5</u>	<u>6</u>	<u>7</u>	<u>8</u>	<u>9</u>	<u>10</u>
1		248.1	248.1	248.1	248.2	248.3	248.5	248.8	249.2	249.9
2	172.2	183.5	206.4	224.6	238.2	247.0	250.5	257.9	267.9	275.7
3	177.6	196.1	227.3	245.5	251.8	266.4	280.9	294.1	304.8	312.8
4	184.7	209.5	242.5	254.4	276.1	297.4	316.7	331.2	341.9	350.0
5		360.8	360.8	360.8	360.9	361.4	363.4	369.6	379.1	387.2

<u>TEMPERATURE, DEGREES FAHRENHEIT</u>										
1		398.8822	398.8827	398.8855	398.8981	398.9423	399.0276	399.1301	399.3082	399.5559
2	366.8782	372.9753	383.0746	389.9853	395.1166	398.4603	399.7671	399.8496	399.8979	399.9522
3	369.8058	379.2011	390.9933	397.9063	399.9886	399.9776	399.9721	399.9694	399.9802	399.9904
4	373.6334	384.2601	396.7470	400.2618	400.2153	400.1472	400.0841	400.0282	399.9943	399.9954
5		400.0292	400.0296	400.0304	400.0311	400.0312	400.0275	400.0141	399.9995	399.9978

<u>STEAM SATURATION</u>										
1		.5693	.5692	.5692	.5686	.5654	.5489	.4935	.3755	.2414
2	.8640	.4688	.3697	.3098	.2471	.1669	.0444	0.0000	0.0000	0.0000
3	.8481	.4225	.2978	.1772	0.0000	0.0000	0.0000	0.0000	0.0000	0.0000
4	.8249	.3840	.2147	0.0000	0.0000	0.0000	0.0000	0.0000	0.0000	0.0000
5		0.0000	0.0000	0.0000	0.0000	0.0000	0.0000	0.0000	0.0000	0.0000

TABLE 7

SUMMARY OF FRACTURED MATRIX RUN CHARACTERISTICS

<u>RUN NO.</u>	<u>PRODUCTION RATE, LBS/HR</u>	<u>TIME STEP, DAYS</u>	<u>TOTAL TIME, DAYS</u>	<u>AVERAGE NUMBER OF ITERATIONS PER STEP</u>	<u>AVERAGE MAXIMUM SATURATION CHANGE/STEP</u>	<u>TOTAL RUN TIME, CDC 6600 CPU SECONDS</u>
1	40	30	1500	5.1	0.38	32.3
2	40	60	1500	8.5	0.66	26.5
3	10	120	4200	4.4	0.31	20.7

TABLE 8

HOT DRY ROCK RESULTS AT 3,000 DAYS
 400 x 400 FEET, 100,000 DARCY FRACTURE

PRESSURE, PSIA					
J = 1					
	1	2	3	4	5
1	801.8	801.7	801.6	801.4	801.0
2	836.1	836.0	835.9	835.7	835.6
3	870.6	870.4	870.3	870.1	870.0
4	905.2	905.0	904.8	904.6	904.5
5	940.2	939.6	939.2	939.0	938.8

TEMPERATURE, °F					
J = 1					
	1	2	3	4	5
1	138.4375	139.1442	139.1278	137.9985	137.4555
2	120.3707	123.2967	126.2684	129.1460	134.0118
3	110.5972	114.3772	118.9110	124.1954	132.1117
4	104.7869	108.3930	113.2686	119.6754	129.3627
5	101.5197	104.4184	108.9581	115.5032	126.0568

J = 2					
	1	2	3	4	5
1	192.0262	192.6029	192.6152	191.7483	191.3081
2	176.3268	178.7883	181.4228	184.0100	187.8308
3	166.5993	169.9373	174.1229	178.9975	185.4905
4	160.7664	164.0263	168.6004	174.5594	182.6227
5	157.5881	160.3054	164.6232	170.7594	179.5778

J = 3					
	1	2	3	4	5
1	429.3812	429.4605	429.4268	429.2234	429.0697
2	425.2453	425.7926	426.4512	427.0833	427.7481
3	421.5898	422.5007	423.7477	425.1202	426.4752
4	419.1658	420.1519	421.6267	423.4105	425.2228
5	417.9100	418.8160	420.2795	422.1785	424.2129

J = 4					
	1	2	3	4	5
1	494.8779	494.8820	494.8786	494.8643	494.8519
2	494.5635	494.6016	494.6501	494.6957	494.7357
3	494.2421	494.3122	494.4119	494.5182	494.6096
4	494.0161	494.0965	494.2197	494.3629	494.4906
5	493.8991	493.9765	494.1023	494.2578	494.4033

J = 5					
	1	2	3	4	5
1	499.9092	499.9092	499.9092	499.9090	499.9088
2	499.9036	499.9042	499.9051	499.9059	499.9065
3	499.8974	499.8986	499.9005	499.9024	499.9039
4	499.8928	499.8943	499.8966	499.8993	499.9014
5	499.8905	499.8919	499.8944	499.8973	499.8998

X-DIRECTION FLOW RATE, LBS/HR

J = 1					
	1	2	3	4	5
1	0.0000	2016.3670	4220.8752	7060.5410	12124.8302
2	0.0000	1894.5775	3315.5218	4256.6210	4316.0297
3	0.0000	2721.4537	3732.2798	3633.6808	2548.8300
4	0.0000	5329.2430	5442.0878	4342.7514	2582.6891
5	0.0000	13038.3583	8289.2342	5706.4035	3427.6178

Z-DIRECTION FLOW RATE, LBS/HR

J = 1					
	1	2	3	4	5
1	0.0000	0.0000	0.0000	0.0000	0.0000
2	-2016.3674	-2204.5087	-2839.6660	-5064.2894	-12875.1657
3	-3910.9451	-3625.4529	-3780.7657	-5123.6984	-8559.1363
4	-6632.3988	-4636.2794	-3682.1667	-4038.8478	-6010.3065
5	-11961.6419	-4749.1240	-2582.8306	-2278.7858	-3427.6175

TABLE 9

HOT DRY ROCK RESULTS AT 75 DAYS
800 x 800 FEET, 800,000 DARCY FRACTURE

PRESSURE, PSIA

J = 1

	1	2	3	4	5
1	800.3	800.3	800.3	800.3	800.2
2	856.7	856.8	856.8	856.8	856.9
3	914.9	914.9	914.8	914.8	914.8
4	975.2	975.3	975.3	975.4	975.4
5	1039.3	1039.2	1039.1	1039.1	1039.0

TEMPERATURE, °F

J = 1

	1	2	3	4	5
1	468.3370	471.2289	474.2237	477.2610	479.9644
2	462.7538	457.2984	452.0257	446.7013	441.5233
3	399.0010	407.6237	416.3509	425.0627	433.5945
4	375.0946	361.0486	347.2332	333.3667	318.6657
5	189.6355	220.9219	247.4867	271.6548	295.6675

J = 2

1	483.8634	485.4144	486.9969	488.4728	489.6844
2	480.5561	477.4840	474.5136	471.6448	469.0360
3	444.7546	449.7848	454.8366	459.6667	464.3795
4	427.2917	419.0025	410.6463	402.3857	394.1028
5	318.5235	336.7667	352.4632	366.8352	380.9695

J = 3

1	498.8198	498.9383	499.0600	499.1664	499.2459
2	498.5441	498.2961	498.0542	497.8271	497.6309
3	495.6178	496.0338	496.4561	496.8485	497.2234
4	493.9525	493.2536	492.5389	491.8334	491.1513
5	484.7310	486.2680	487.6116	488.8412	490.0439

J = 4

1	499.9913	499.9922	499.9931	499.9939	499.9944
2	499.9891	499.9871	499.9852	499.9835	499.9820
3	499.9650	499.9693	499.9726	499.9757	499.9786
4	499.9520	499.9464	499.9407	499.9350	499.9296
5	499.8779	299.8902	499.9011	499.9110	499.9207

J = 5

1	500.0000	500.0000	500.0000	500.0000	500.0000
2	500.0000	500.0000	500.0000	500.0000	500.0000
3	499.9999	500.0000	500.0000	500.0000	500.0000
4	499.9999	499.9999	499.9999	499.9999	499.9999
5	499.9998	499.9998	499.9998	499.9999	499.9999

X-DIRECTION FLOW RATE, LBS/HR

J = 1

	1	2	3	4	5
1	0.0000	20882.9777	23901.9082	24797.3057	24949.6943
2	0.0000	-23698.1287	-27798.6156	-28338.0482	-26240.1155
3	0.0000	25170.5939	29614.1274	29702.3133	26689.1928
4	0.0000	-28661.3533	-32354.1902	-32389.5505	-28477.6646
5	0.0000	31305.4018	31635.7540	31226.4479	28076.8419

Z-DIRECTION FLOW RATE, LBS/HR

J = 1

	1	2	3	4	5
1	0.0000	0.0000	0.0000	0.0000	0.0000
2	-20883.0478	-3018.9908	-895.4625	-152.4403	-47.8279
3	2815.0301	1081.4271	-356.1100	-2250.4732	-26288.0461
4	-22355.7438	-3362.2535	-444.4305	762.5207	401.0460
5	6305.5481	330.4875	-409.1554	-3149.4712	-28076.7050

TABLE 10

HOT DRY ROCK RESULTS AT 3,000 DAYS
800 x 800 FEET, 800,000 DARCY FRACTURE

PRESSURE, PSIA

J = 1

	1	2	3	4	5
1	800.5	800.5	800.5	800.5	800.4
2	866.5	866.5	866.5	866.5	866.5
3	933.3	933.4	933.4	933.4	933.4
4	1000.9	1000.9	1000.9	1001.0	1001.0
5	1069.4	1069.3	1069.2	1069.1	1069.1

TEMPERATURE, °F

J = 1

	1	2	3	4	5
1	249.9689	248.0220	246.8849	245.8461	244.6164
2	216.5695	218.9366	219.5740	219.3443	218.4954
3	194.9029	190.9242	188.9332	188.3424	188.9908
4	153.6767	160.1790	163.8029	164.3298	161.8779
5	106.4226	113.7653	122.3591	132.9277	147.4336

J = 2

1	265.8360	263.9998	262.9122	261.9491	260.8865
2	233.9842	236.1508	236.7515	236.5108	235.6197
3	212.3962	208.7877	206.9809	206.5027	207.2386
4	172.9634	178.9138	182.1814	182.5563	180.1299
5	126.2235	133.4061	141.8190	152.1030	165.9797

J = 3

1	324.7246	323.3435	322.4850	321.8252	321.3318
2	299.2753	300.7499	301.1835	300.8914	299.8991
3	279.0948	276.7346	275.5776	275.4845	276.4692
4	246.9943	251.0076	253.0511	252.9464	250.6793
5	204.0660	210.4347	217.8984	226.8161	238.1241

J = 4

1	451.0672	450.7327	450.5302	450.4661	450.5618
2	443.0764	443.3598	443.3921	443.1553	442.6485
3	434.2412	433.8323	433.7200	433.9624	434.5498
4	423.0384	423.8462	424.1298	423.7657	422.7861
5	404.4443	407.1044	410.1953	413.6774	417.5579

J = 5

1	497.0347	497.0183	497.0098	497.0131	497.0286
2	496.5171	496.5274	496.5235	496.5012	496.4625
3	496.8260	495.8133	495.8179	495.8454	495.8922
4	495.0225	495.0594	495.0655	495.0298	494.9592
5	493.5814	493.7861	494.0234	494.2813	494.5475

X-DIRECTION FLOW RATE, LBS/HR

J = 1

	1	2	3	4	5
1	0.0000	3823.3153	8511.9081	13606.8777	19054.8352
2	0.0000	2706.8557	2765.7626	2153.8488	1207.0827
3	0.0000	-3422.8521	-3693.5112	-2396.7712	-729.3971
4	0.0000	214.0614	-935.5022	-3068.0366	-4893.8505
5	0.0000	21678.6244	18351.3309	14704.0595	10361.3012

Z-DIRECTION FLOW RATE, LBS/HR

J = 1

	1	2	3	4	5
1	0.0000	0.0000	0.0000	0.0000	0.0000
2	-3823.8456	-4688.5961	-5094.9711	-5447.9598	-5945.1321
3	-6530.4336	-4748.0656	-4483.0575	-4501.1982	-4738.0462
4	-3107.2900	-4477.0181	-5779.8014	-6168.5727	-5467.4493
5	-3321.3739	-3327.2930	-3647.2701	-4342.7575	-10361.3018

FIGURE 1
 DELIVERABILITY FACTOR f VS. P_w FOR RELATIVE PERMEABILITY
 CURVES OF EQN (26)

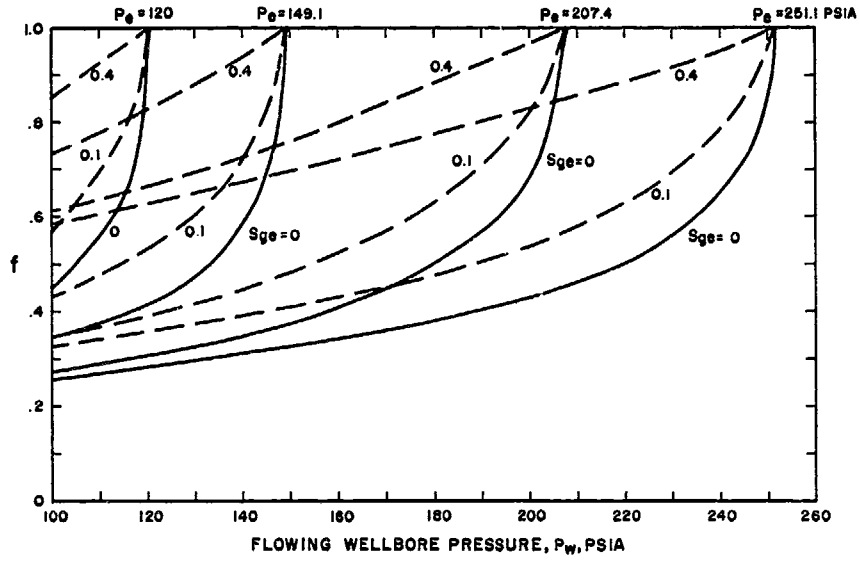


FIGURE 2
 PRODUCTION RATE VS. S_{ge} FOR RADIAL
 WATER-STEAM FLOW

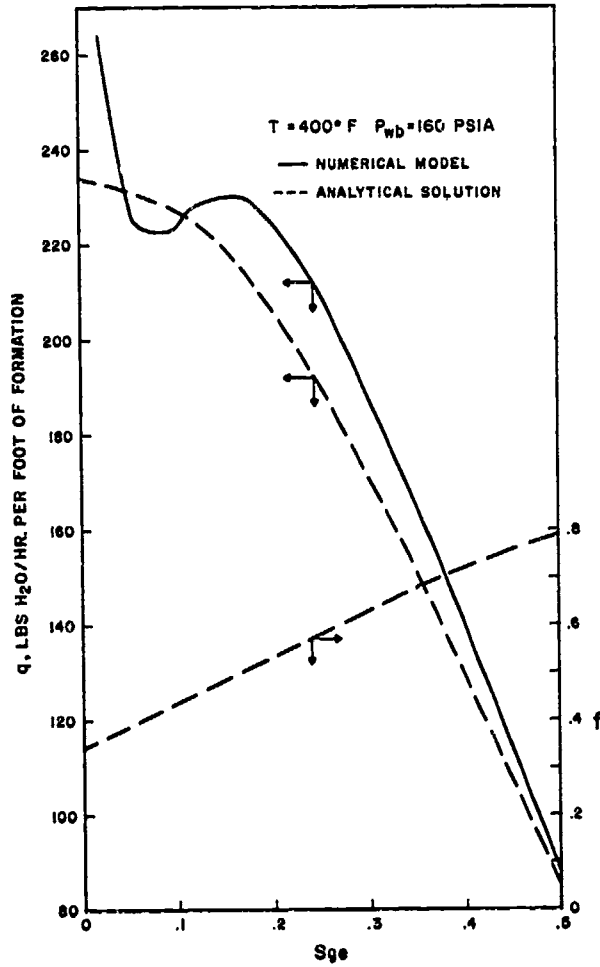


FIGURE 3
TIME TRUNCATION ERROR

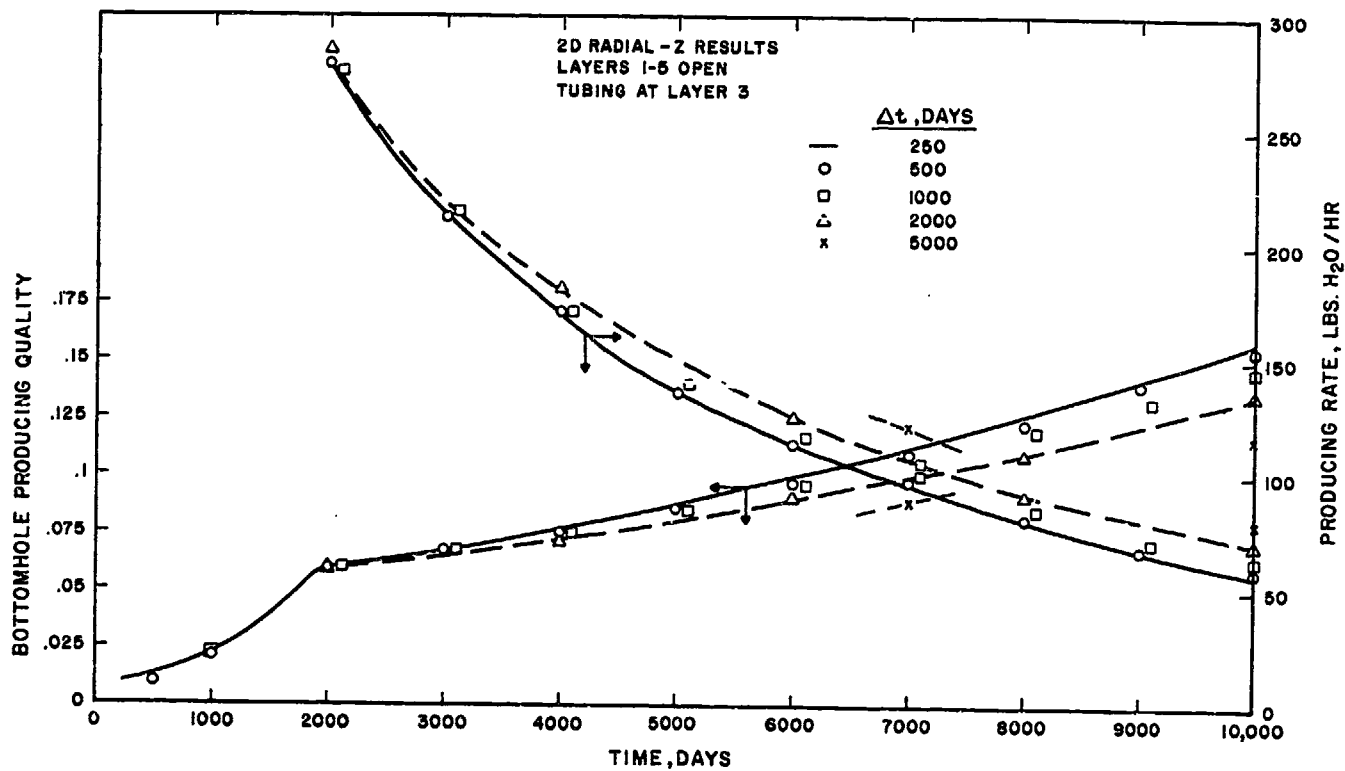


FIGURE 4
EFFECT OF PERMEABILITY ON PRODUCTION RATE AND QUALITY

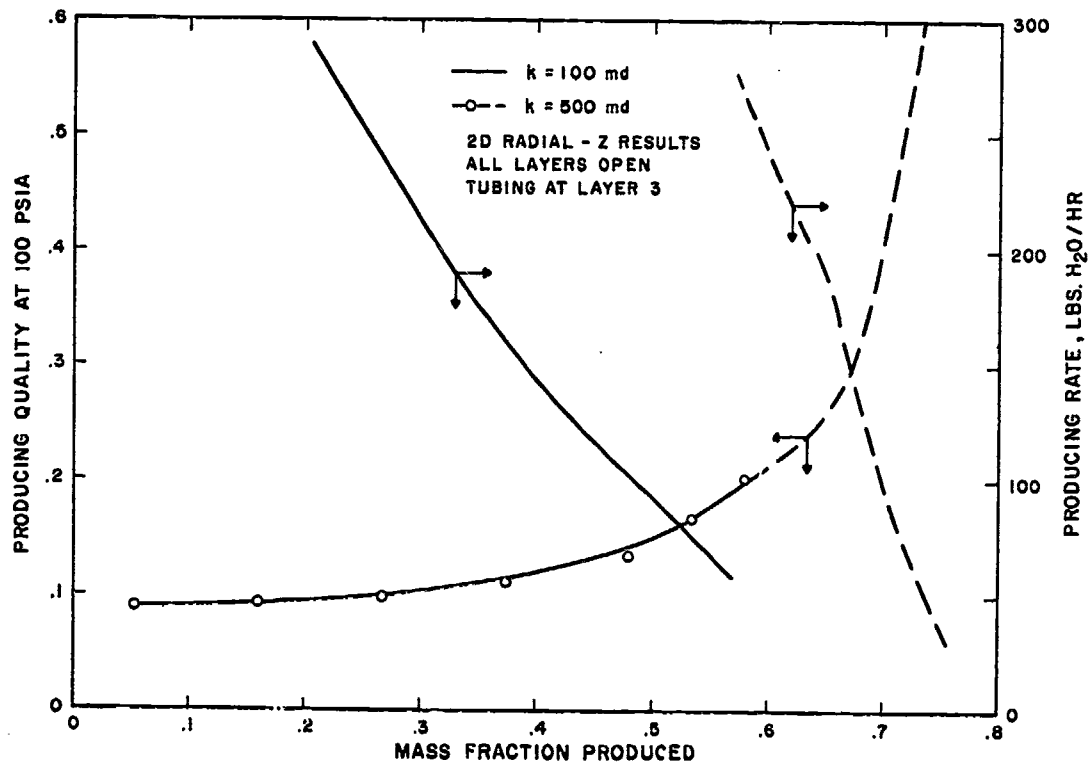


FIGURE 5
EFFECT OF PERMEABILITY AND POROSITY ON
AVERAGE RESERVOIR PRESSURE DECLINE

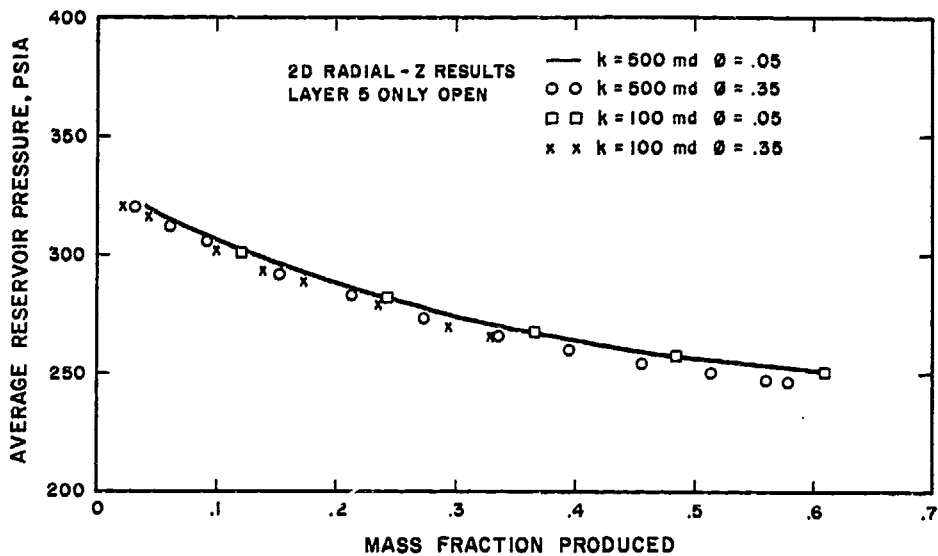


FIGURE 6
RADIAL-Z GRID FOR MATRIX-FISSURE SYSTEM

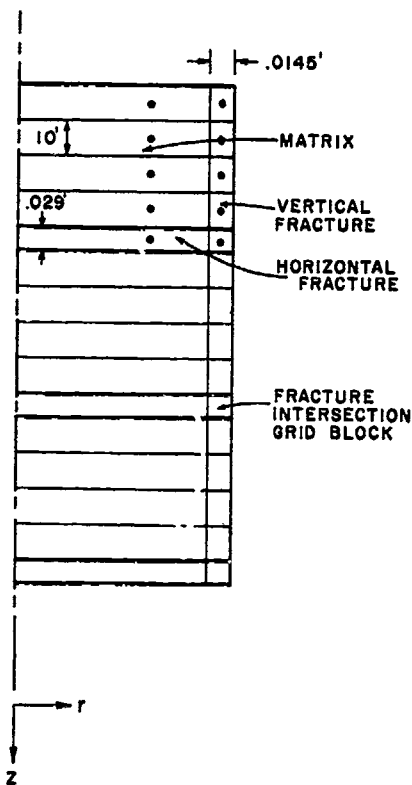


FIGURE 7
MATRIX-FISSURE SIMULATION RESULTS
AT 1500 DAYS

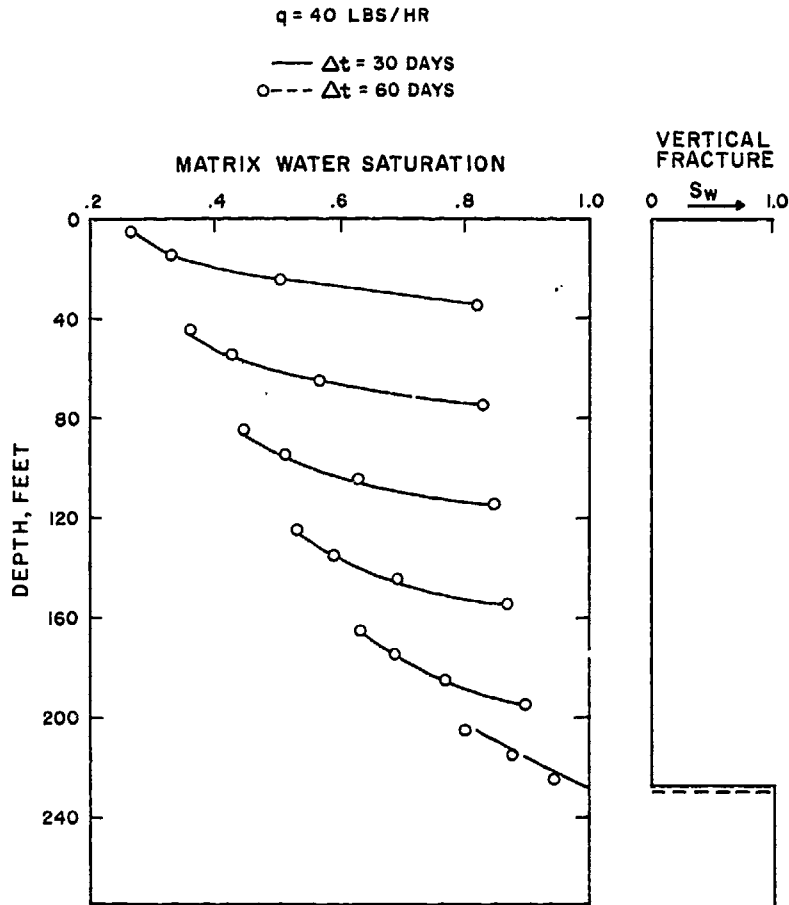


FIGURE 8
EFFECT OF PRODUCTION RATE ON
MATRIX-FISSURE SIMULATION RESULTS

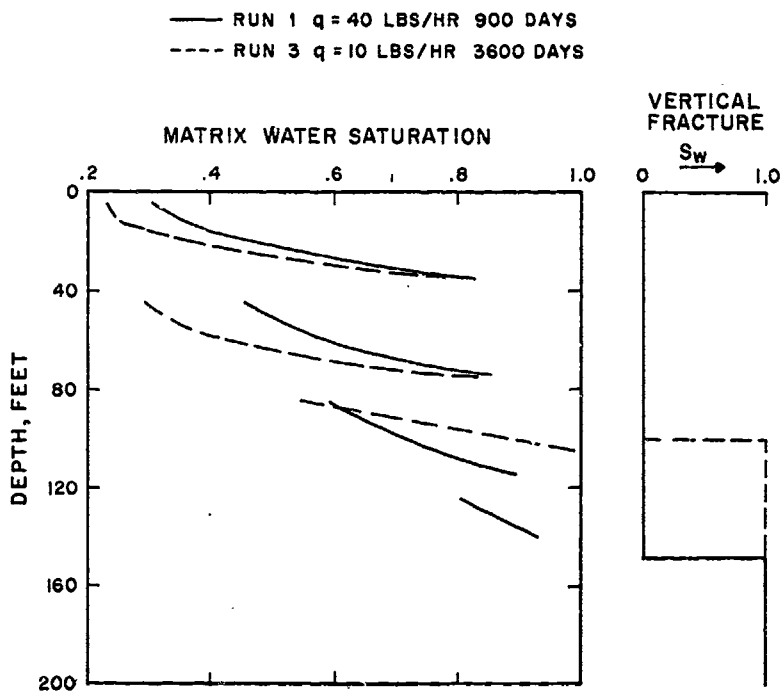


FIGURE 9
COMPARISON OF MATRIX-FISSURE AND
CONVENTIONAL SIMULATION RESULTS

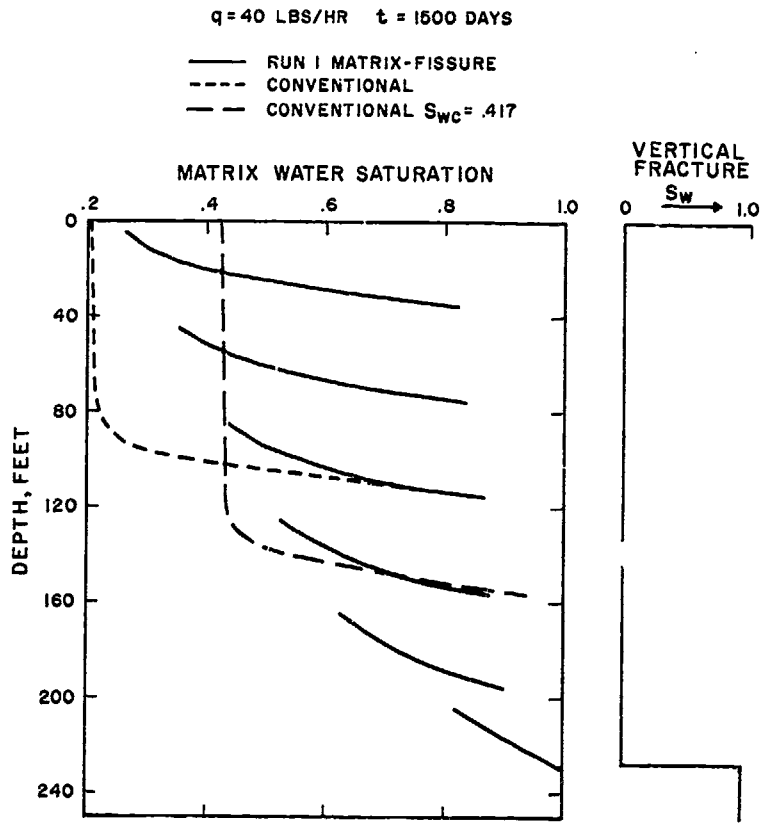


FIGURE 10
CALCULATED PRESSURE DRAWDOWN, Δp VS. TIME

HORIZONTAL FRACTURE SPACING = 44 FT.
 RATE = 10,000 LBS/HR

RUN	FRACTURE		MATRIX PERMEABILITY, MD
	k _w , DARCY-FT.	w, MM	
1	4	.245	.0001
2	4	.245	.001
3	4	.245	.01
4	HOMOGENEOUS, k = 90.9 MD		
5	546.4	1.26	.0001

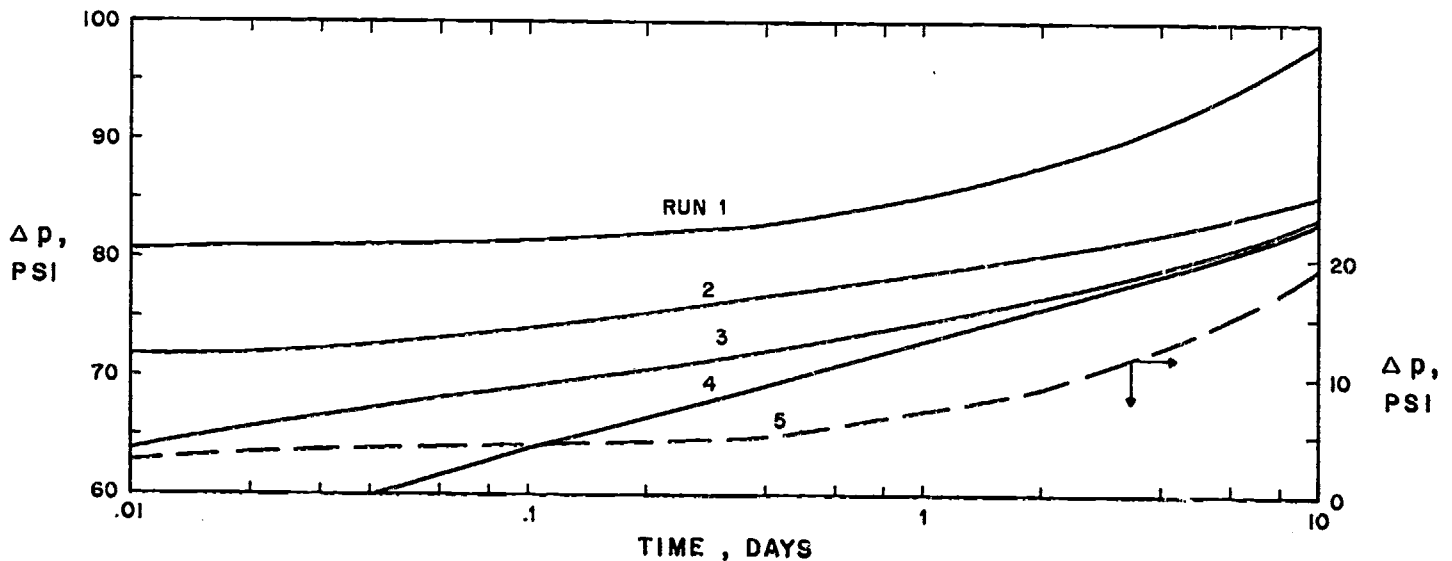


FIGURE 11
CALCULATED PRESSURE DRAWDOWN, Δp VS. TIME

HORIZONTAL FRACTURE SPACING = 440 FT.
 RATE = 100,000 LBS/HR

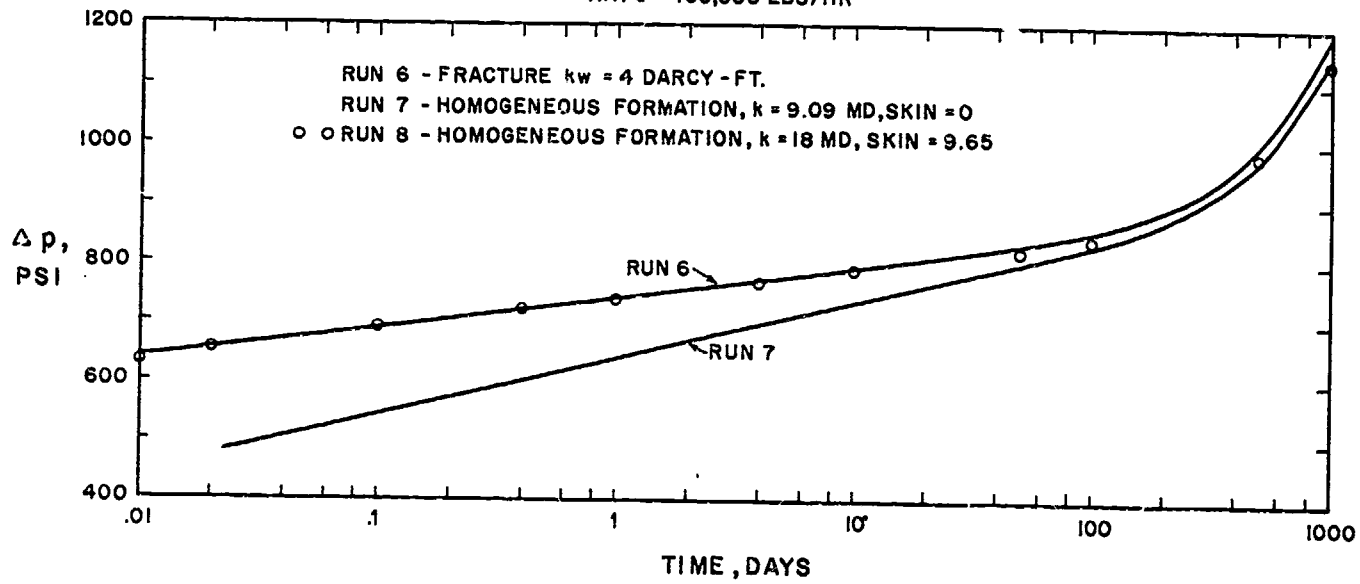


FIGURE 12
CALCULATED ENERGY RECOVERY AND PRODUCED WATER TEMPERATURE VS. TIME FOR HOT DRY ROCK SYSTEM

